bioRxiv preprint doi: https://doi.org/10.1101/2021.03.04.434028; this version posted March 5, 2021. The copyright holder for this preprint (which was not certified by peer review) is the author/funder. All rights reserved. No reuse allowed without permission.

1

2 Molecular mechanism regulating transcriptional control of the *hig* 3 toxin-antitoxin locus of antibiotic-resistance plasmid Rts1 from 4 *Proteus vulgaris*

5

6 Ian Pavelich[1,2], Marc A. Schureck[1], Dongxue Wang[1], Eric D. Hoffer[1], Michelle Boamah[1],

7 Nina Onuoha[1], Stacey J. Miles[1], C. Denise Okafor[3], and Christine M. Dunham[1]*

8

9 [1]Department of Biochemistry and the Emory Antibiotic Resistance Center, Emory

10 University School of Medicine, Atlanta, Georgia, 30322

11 [2]Department of Chemistry, Emory University, Atlanta, Georgia, 30322

12 [3]Department of Biochemistry and Molecular Biology, Pennsylvania State University,

13 University Park, Pennsylvania 16802

14

15 These authors contributed equally.

16 *To whom correspondence should be addressed: Tel: 1-404-712-1756; Fax: 1-404-727-

17 2738; Email: christine.m.dunham@emory.edu

18 Data deposition: Crystallography, atomic coordinates, and structure factors have been

19 deposited in the Protein Data Bank, www.pdb.org (PDB codes 6W6U, 6WFP)

20

21 **Running title:** Regulation of *P. vulgaris* HigBHigA toxin-antitoxin

22

23 **Keywords:** toxin-antitoxin complexes, gene expression regulation, transcriptional

24 repression, DNA-binding proteins, X-ray crystallography, *Proteus vulgaris*

bioRxiv preprint doi: https://doi.org/10.1101/2021.03.04.434028; this version posted March 5, 2021. The copyright holder for this preprint (which was not certified by peer review) is the author/funder. All rights reserved. No reuse allowed without permission.

25 **ABSTRACT**

26 Regulation of ubiquitous bacterial type II toxin-antitoxin (TA) gene pairs occurs via a negative
27 feedback loop whereby their expression is typically responsive to changing levels of toxins
28 at the transcriptional level similar to a molecular rheostat. While this mechanism can explain
29 how certain TA complexes are regulated, accumulating evidence suggests diversity in this
30 regulation. One system for which the negative feedback loop is not well defined is the
31 plasmid-encoded HigBHigA TA pair originally identified in a post-operative infection with
32 antibiotic resistant *Proteus vulgaris*. In contrast to other type II TA modules, each *hig*
33 operator functions independently and excess toxin does not contribute to increased
34 transcription *in vivo*. Structures of two different oligomeric complexes of HigBHigA bound to
35 its operator DNA reveal similar interactions are maintained suggesting plasticity in how *hig*
36 is repressed. Consistent with this result, molecular dynamic simulations reveal both
37 oligomeric states exhibit similar dynamics. Further, engineering a dedicated trimeric
38 HigBHigA complex does not regulate transcriptional repression. We propose that HigBHigA
39 functions via a simple on/off transcriptional switch regulated by antitoxin proteolysis rather
40 than a molecular rheostat. The present studies thus expand the known diversity of how these
41 abundant bacterial protein pairs are regulated.

42

43

44

45

46

47

48

49

bioRxiv preprint doi: https://doi.org/10.1101/2021.03.04.434028; this version posted March 5, 2021. The copyright holder for this preprint (which was not certified by peer review) is the author/funder. All rights reserved. No reuse allowed without permission.

IMPORTANCE

Bacteria respond to various stimuli by rapidly regulating gene expression to control growth. The diversity in how bacteria inhibit growth is exemplified by the abundance and diversity of toxin-antitoxin (TA) gene pairs. To tightly regulate their own expression, antitoxin proteins function as transcriptional autorepressors with additional regulation imparted by responsiveness of the system to toxin concentrations, similar to a molecular rheostat. However, some TAs do not appear to be responsive to changing levels of toxin. To expand our understanding of diverse TAs, we studied the regulation of a structurally distinct TA called host inhibition of growth (HigBA) originally discovered on the antibiotic resistance Rts1 plasmid associated with *Proteus vulgaris*. We find that the *hig* operon is regulated via a simple on/off transcriptional switch that is incalcitrant to changing toxin levels. These results expand the known mechanistic diversity of how TA pairs regulate their expression.

bioRxiv preprint doi: https://doi.org/10.1101/2021.03.04.434028; this version posted March 5, 2021. The copyright holder for this preprint (which was not certified by peer review) is the author/funder. All rights reserved. No reuse allowed without permission.

75 **INTRODUCTION**

76 Bacterial toxin-antitoxin (TA) genes are bicistronic operons found in mobile genetic elements
77 and bacterial chromosomes (1-3). Type II TA modules consist of toxin and antitoxin protein
78 components that form architecturally diverse macromolecular complexes in the absence of
79 external stimuli and during nutrient-rich growth. Although these gene pairs were first
80 identified on plasmids and in bacteriophages (4-9), TAs are highly abundant in free-living
81 bacteria where they appear to have different functions. In their role in plasmid maintenance,
82 the toxin component can induce post-segregational killing if both genes are not inherited (6).
83 In the past few years, conflicting experimental data on the endogenous activities of TAs have
84 led to ambiguity and controversy surrounding their roles in bacterial physiology (10).

85 Regulation of type II TA pairs frequently occurs at the transcriptional level via a
86 negative feedback loop (10-12). Antitoxin proteins contain a DNA-binding motif and repress
87 at operator sites that overlap with promoters of TA genes. Toxin proteins are either recruited
88 to their cognate antitoxins bound at these operator sites or bind to operators as TA
89 complexes where they function as co-repressors, allowing the system to be responsive to
90 changes in toxin expression levels. Further, TAs can form different oligomeric complexes
91 when bound at operator sites that alter their binding thermodynamics to result in a gradient
92 of the transcriptional response similar to a molecular rheostat (13, 14). This response
93 gradient can also be influenced by cooperative TA binding at adjacent operator sites; this
94 process is known as "conditional cooperativity" (15-18). However, this model is dependent
95 on the architectural organization of TAs pairs which can diverge significantly (12, 19). Thus,
96 it is unclear if conditional cooperativity can explain the regulation of all type II TA systems.

97 The structural diversity and distinct toxin- and DNA-binding motifs of different type II
98 antitoxin proteins may partially explain why they can exert different mechanisms of
99 autoregulation (11). Antitoxins contain ribbon-helix-helix (RHH), helix-turn-helix (HTH),

bioRxiv preprint doi: https://doi.org/10.1101/2021.03.04.434028; this version posted March 5, 2021. The copyright holder for this preprint (which was not certified by peer review) is the author/funder. All rights reserved. No reuse allowed without permission.

100 Phd/YefM or SpoVT/AbrB DNA-binding motifs, with RHH and HTH being the most common
101 (20-26). The type of DNA binding motif affects transcriptional repression. HTH-containing
102 antitoxins contain a complete DNA-binding motif while RHH-containing antitoxins contain a
103 half site requiring antitoxin dimerization for DNA binding. TA operons usually contain multiple
104 operator sites and antitoxin binding at adjacent sites can lead to cooperativity and an
105 increase in transcriptional repression (17, 18, 27). Antitoxins are particularly susceptible to
106 proteases especially during changing cellular conditions (28). This reduction in antitoxin
107 concentration increases free toxin levels that when free, can inhibit growth. Free toxin can
108 also interact with antitoxins bound at their operators changing the oligomeric state of the TA
109 complex during repression. These oligomeric state changes, in turn, can lead to differences
110 in the ability of TAs to bind their operator and influence the extent of repression; effectively
111 this responsiveness allows the system to function as a molecular rheostat (**Fig. 1**). In
112 contrast, other TA systems do not appear to be responsive to changing levels of toxin and
113 instead are simple on/off transcriptional switches (29, 30). While there exists some
114 experimental evidence that distinguishes between the molecular rheostat and the on/off
115 switch modes of regulation, at present the molecular basis for each mechanism is
116 ambiguous because there is little or no structural evidence as a foundation for each model.

117 The *host inhibition of growth* BA (*higBA*) TA module seems to function as an on/off
118 switch. The HigBHigA pair was first identified on the antibiotic-resistance plasmid Rts1
119 associated with *Proteus vulgaris* and discovered post-operatively in an urinary tract infection
120 (31, 32) (we call this TA pair "HigBHigA" to denote both the HigB toxin and HigA antitoxin
121 proteins). The HigB toxin belongs to the RelE family of toxins, resembles a microbial
122 ribonuclease and cleaves mRNA substrates bound to a translating ribosome (26, 33-35).
123 Although there are HigBHigA TA pairs found chromosomally and these HigB toxins are also
124 RelE family members (36, 37), the structural organization and the regulation of these

bioRxiv preprint doi: https://doi.org/10.1101/2021.03.04.434028; this version posted March 5, 2021. The copyright holder for this preprint (which was not certified by peer review) is the author/funder. All rights reserved. No reuse allowed without permission.

125 systems compared to the *P. vulgaris* associated module seems to be different (26). While
126 all known HigA homologs contain a HTH DNA-binding motif, the *P. vulgaris* associated
127 antitoxin binds to each of its operator sites (O1 and O2) in a non-cooperative manner (26,
128 38). Here, we test the two models of transcriptional regulation, rheostat versus on/off switch,
129 to determine the molecular mechanism of action of HigBHigA.
130

131 ## RESULTS

132 **Transcriptional repression at each operator is independently regulated.** The *hig*
133 promoter (P*hig*) is negatively autoregulated by the HigBHigA complex binding at operators
134 O1 and O2 that overlap with the -35 and -10 promoter sites (32) (**Fig. 2A**). The HigBHigA
135 complex forms a tetrameric assembly with two HigB monomers and a HigA dimer
136 ($HigB_2HigA_2$) (26). Each HigA antitoxin contains a single HTH DNA-binding motif and forms
137 an obligate dimer, meaning that two HigA antitoxins in one $HigB_2HigA_2$ complex bind two
138 inverted repeats of a single DNA operator (26, 38). To determine if we could build oligomeric
139 complexes *in vitro*, we monitored the binding of the $HigB_2HigA_2$ complex to *hig* (O1 and O2)
140 using an electrophoretic mobility shift assay (EMSA) (**Fig. 2B**). The $HigB_2HigA_2$ complex
141 was purified according to previously published protocols and the DNA probe used in the
142 EMSA consists of the entire 61 basepair (bp) operator region (**Table S1**). Titration of
143 $HigB_2HigA_2$ with a constant amount of *hig* causes two molecular weight shifts, indicating
144 binding of $HigB_2HigA_2$ at each operator site (**Fig. 2B**, top). To determine whether $HigB_2HigA_2$
145 binds with a higher affinity to either O1 or O2, all 21 nucleotides in each operator were
146 randomized individually (38). Each of these 21 nucleotides located in either O1 or O2 were
147 previously shown to be protected upon HigA binding (39). Therefore any change in the
148 mobility of the DNA band using a scrambled O1 or O2 would represent binding of $HigB_2HigA_2$
149 to a single operator. $HigB_2HigA_2$ binds to each of the two sites represented as a single

bioRxiv preprint doi: https://doi.org/10.1101/2021.03.04.434028; this version posted March 5, 2021. The copyright holder for this preprint (which was not certified by peer review) is the author/funder. All rights reserved. No reuse allowed without permission.

150 molecular weight shift and both result in similar dissociation binding constants (0.36 ± 0.09
151 μM for O1 and 0.24 ± 0.04 μM for O2) (**Fig. 2B**, middle and lower; **Table S2**). These data
152 indicate that $HigB_2HigA_2$ recognizes each operator independently to form a high affinity
153 interaction. This observation appears to be an important distinction from other type II TAs
154 where TA complexes binding at an operator influences the binding of TAs at adjacent
155 operators (**Fig. 1**).

156 To test whether $HigB_2HigA_2$ binding at a single operator results in transcriptional
157 repression *in vivo*, we designed a series of constructs that encode *lacZ* in three different
158 contexts: downstream of the P*hig* promoter (pQF50-P*hig*-*lacZ*), downstream of wild-type
159 HigA (pQF50-P*hig*-*higA*-*lacZ*), or downstream of a C-terminally truncated HigA (pQF50-
160 P*hig*-*higA*(∆84-104)-*lacZ*) (**Fig. 2C**). The pQF50-P*hig*-*lacZ* construct reports on the activity
161 of P*hig* in the absence of repressor HigA, while the HigA-encoding pQF50-P*hig*-*higA*-*lacZ*
162 construct reports on how expression of HigA represses P*hig*. The third construct serves as
163 a control as the HigA(∆84-104) variant is unable to dimerize and bind P*hig* but is comparably
164 expressed (26, 38). P*hig*-*lacZ* shows robust β-galactosidase (β-gal) activity which we
165 normalize to represent complete transcriptional repression (this is represented as 0%
166 repression; **Fig. 2C**). Expression of HigA efficiently represses P*hig*, whereas HigA(∆84-104)
167 restores P*hig* activity to near P*hig*-only levels, indicating transcriptional repression is
168 dependent on HigA expression and dimerization (**Fig. 2C**). To test whether $HigA_2$ binding to
169 a single operator region is sufficient for repression, we mutated either O1 or O2 recognition
170 sequences important for HigA binding (38) and repeated the previously described β-gal
171 assays. Mutations to either O1 ($G_{-24}T/C_{-30}A$) or O2 ($G_{-8}T/C_{-2}A$) do not affect $HigA_2$ repression
172 at a single mutant P*hig* when compared to the wild-type P*hig* (**Fig. 2C**, compare middle bars
173 in “O1 variant” and “O2 variant” group to “P*hig*”). These results show that $HigA_2$ binding at
174 either O1 or O2 is sufficient for repression (data also presented in Miller Units in **Fig. S1**).

bioRxiv preprint doi: https://doi.org/10.1101/2021.03.04.434028; this version posted March 5, 2021. The copyright holder for this preprint (which was not certified by peer review) is the author/funder. All rights reserved. No reuse allowed without permission.

175 Further, these data indicate that $HigA_2$ binding at each *hig* operator is not cooperative, and
176 that a single operator is sufficient for transcriptional repression.
177

178 **Addition of HigB destabilizes interactions between HigA and DNA *in vitro*.** The
179 expression of most type II TA complexes is regulated at the transcriptional level by changing
180 toxin and antitoxin concentrations as a result of increased proteolysis of the antitoxin during
181 external stimuli (17, 18, 22). We reasoned that the HigBHigA complex may transcriptionally
182 repress using a different mechanism because of the structural diversity of the HigA antitoxin.
183 The unique structure of HigA could influence its interactions with *hig* or HigB toxin binding.
184 For example, the HigA HTH motif is a complete DNA-binding domain and by extension, the
185 obligate $HigA_2$ dimer contains two DNA-binding domains. Other type II antitoxins typically
186 contain a single DNA-binding motif formed by antitoxin dimerization (**Fig. 1**). These
187 differences are likely important for the changing of different oligomeric TA complexes bound
188 to operators allowing the system to respond to changing toxin levels. To test this, we
189 explored whether the presence of excess HigB changes the molecular interactions of HigA
190 with the O1-O2 operators (**Fig. 3**). Addition of $HigA_2$ to O1-O2 results in two shifted bands
191 of lower mobility, indicative of complexes with a single $HigA_2$ dimer bound to one operator
192 (**Fig. 3A**, **yellow**), or two $HigA_2$ dimers binding to each operator (**Fig. 3A, orange**).
193 Increasing amounts of HigB results in the formation of two additional higher molecular weight
194 species (**Fig. 3A**). In this case, either the HigB monomer binds to each of the $HigA_2$ dimers
195 to form a trimeric $HigBHigA_2$ complex (**Fig. 3A, red**) or both HigB monomers bind to a single
196 $HigA_2$ dimer as a tetrameric $HigB_2HigA_2$ (**Fig. 3A, purple**). As the $HigA_2$ dimer is already
197 bound at both O1 and O2, it is unlikely that the molecular weight species would represent
198 occupation of only a single operator site. While the third shift may contain a mixed population
199 of oligomeric states where HigB binds only one $HigA_2$ dimer (**Fig. 3A, red**), an additional

bioRxiv preprint doi: https://doi.org/10.1101/2021.03.04.434028; this version posted March 5, 2021. The copyright holder for this preprint (which was not certified by peer review) is the author/funder. All rights reserved. No reuse allowed without permission.

200 observable migration shift may be difficult to observe. Thus, we assume the slowest
201 migrating band is a tetrameric $HigB_2HigA_2$-O1-O2 complex. When the molar ratio of HigB to
202 HigA exceeds one (two HigB monomers to one $HigA_2$ dimer or 1.0 μM HigB for 0.5 μM $HigA_2$
203 dimer), only free DNA is observed suggesting that excess HigB destabilizes the association
204 between HigA and DNA. These results appear to be similar to what has been observed with
205 other type II TA complexes that exhibit regulation via conditional cooperativity (17, 18, 27).

206 To determine whether the instability of the HigBHigA complex with O1-O2 is
207 dependent upon the occupancy of both O1 and O2, we next tested complex formation on
208 DNA containing either a scrambled O1 or O2 to prevent $HigA_2$ binding (same mutation as
209 used in Fig. 2). Addition of $HigA_2$ to DNA containing either a scrambled O1 or O2 results in
210 a slower moving species indicative of the $HigA_2$ dimer binding at one operator (**Fig. 3C,**
211 **orange**). Increasing amounts of HigB shows a single, slower moving molecular weight
212 species (**Fig. 3C, purple**). At this point, we assume the HigBHigA complex is tetrameric
213 ($HigB_2HigA_2$) given the prior crystal structures (26). Once the HigB to HigA molar ratio almost
214 exceeds 1 (i.e. 1.0 μM HigB for 0.5 μM $HigA_2$ dimer), the complex is unstable and DNA is
215 released. Interestingly, in the context of both O1 and O2 (**Fig. 3A**), the molar ratio of HigB
216 to HigA needs to exceed 1 however, when only one operator is available, this release of
217 DNA occurs at slightly less then 1 molar equivalents of HigB and HigA. Therefore, the
218 instability of HigBHigA binding a single operator appears to be accelerated in the absence
219 of an adjacent HigBHigA complex.

220

221 **Structure of $HigB_2HigA_2$-O2 DNA**. To determine how HigBHigA interacts with its operator
222 DNA, we pursued a high-resolution X-ray crystal structure of HigBHigA bound to a single
223 operator, O2. We performed crystallization trials using two HigBHigA constructs: a six
224 histidine (His_6) affinity tag located at the N terminus of HigB and a His_6 affinity tag located at

bioRxiv preprint doi: https://doi.org/10.1101/2021.03.04.434028; this version posted March 5, 2021. The copyright holder for this preprint (which was not certified by peer review) is the author/funder. All rights reserved. No reuse allowed without permission.

225 the C terminus of HigA. Both HigBHigA variants crystallized in the same condition, however,
226 each resulted in a different oligomeric state of the HigBHigA complex bound to O2. The
227 HigBHigA-His$_6$-O2 complex crystalized in the monoclinic space group C121, was determined
228 to 2.4 Å resolution by single wavelength anomalous diffraction phasing and contained a
229 HigA$_2$ dimer bound to two HigB monomers (**Fig. 4**). The His$_6$-HigBHigA-O2 complex
230 crystalized in the tetragonal space group I4$_1$, was determined by molecular replacement
231 using the previously determined HigA$_2$ model (PDB code 6CF1) to 2.8 Å resolution and
232 contained a HigA$_2$ dimer bound to a single HigB (**Fig. 5**; **Table S3**). In both structures,
233 residues 1–91 were built for each HigB monomer (92 total residues) and all nucleotides (1–
234 21) were built for the O2 DNA duplex (**Fig. S2**). Residues 1–101 and 1–102 in the
235 HigB$_2$HigA$_2$ structure and residues 1–91 and 1–95 in the HigBHigA$_2$ structure were modeled
236 (104 total residues) (**Fig. S2**).

237 The HTH motif in HigA consists of α2, loop 3 and α3 and this region interacts with the
238 major groove of the operator O2 DNA (**Fig. 4A**). In the tetrameric HigB$_2$HigA$_2$-O2 structure,
239 HigA contacts the T$_{-1}$, G$_{-2}$, T$_{-3}$, A$_{-4}$ O2 sequence on the *hig* negative strand (38) (**Figs. 4A, B**).
240 HigA residue Arg40 interacts with the Hoogsteen face of G$_{-2}$ to make the only sequence-
241 specific protein-DNA contact. Residues Thr34 and Thr37 (from α3) contact the phosphate of
242 G$_{+7}$ while the sidechains of Ser23 (from loop 2), Ser39 (from α3), and Lys45 (from α3) are
243 all within hydrogen bonding distance of nucleotides T$_{-7}$, A$_{-6}$, T$_{-5}$, and T$_{-4}$, respectively which
244 are located on the opposite DNA strand (**Fig. S3**). Additionally, Ala36 and Thr34 form van
245 der Waals interactions with the nucleobase C5 methyl of A$_{-3}$. These interactions are similar
246 to those previously observed in the HigA$_2$-O2 DNA interaction (38) and are also present
247 between HigA and O2 on the opposite strand, indicating that HigB binding to form the
248 tetrameric HigB$_2$HigA2-O$_2$ complex does not change interactions of HigA$_2$ with O2.

bioRxiv preprint doi: https://doi.org/10.1101/2021.03.04.434028; this version posted March 5, 2021. The copyright holder for this preprint (which was not certified by peer review) is the author/funder. All rights reserved. No reuse allowed without permission.

249 The termini of antitoxins are typically intrinsically disordered contributing to their
250 proteolysis during external stimuli. In the free $HigA_2$ structure (38), the N terminus is
251 disordered (**Fig. S4A,B**). Upon HigB binding, the HigA termini becomes ordered both in the
252 free $HigB_2HigA_2$ structure (26) and upon binding DNA ($HigB_2HigA_2$-O2 DNA) (**Fig. 4C; Fig.**
253 **S4C,D**). The N- and C-termini of HigA form intramolecular interactions in addition to
254 interactions with α1 of an adjacent HigB in the crystal lattice (**Fig. S4A,B**). Specifically, N-
255 terminal residues Arg2 (side chain) and Gln3 (backbone carbonyl) form salt bridges with C-
256 terminal residues Glu80 and Arg77, respectively, and these interactions presumably stabilize
257 the termini. Thus, binding of HigB stabilizes HigA both in the presence or absence of DNA.
258 Comparison of the overall architecture of $HigB_2HigA_2$-O2 DNA to $HigB_2HigA_2$ (26) or
259 $HigA_2$ (38) reveals subtle changes that may be important for O2 DNA binding and
260 transcriptional repression. Aligning analogous HigA monomers from the $HigB_2HigA_2$-O2 and
261 the $HigB_2HigA_2$ structures (PDB code 4MCX) reveals a ~14° displacement of the adjacent,
262 second HigA protomer (**Fig. 4D**). Similarly, comparison of the free $HigA_2$ dimer (PDB code
263 6CF1) to $HigB_2HigA_2$-O2 also shows rotation of HigA upon DNA binding, although the
264 movement is not as large as compared to when HigB is present (~8° rotation versus a ~14°
265 rotation) (**Fig. S5**). Thus, $HigA_2$ reorients to bind DNA and HigB binding to a $HigA_2$-DNA
266 complex minimally influences the protein-DNA interface.
267
268 **Structure of $HigBHigA_2$-O2 DNA.** As noted above, both the tetrameric $HigB_2HigA_2$-O2 DNA
269 and trimeric $HigBHigA_2$-O2 DNA crystal forms formed in the same crystallization conditions
270 and resulted in two different macromolecular structures (**Table S3**). Interestingly, not all of
271 the interactions seen in tetrameric $HigB_2HigA_2$-DNA are conserved in the trimeric $HigBHigA_2$-
272 O2 structure. While critical interactions of HigA with the T_{-1}, G_{-2}, T_{-3}, A_{-4} recognition sequence
273 are maintained, α2 and α3 of the HTH DNA-binding motif slightly moves away from O2, no

bioRxiv preprint doi: https://doi.org/10.1101/2021.03.04.434028; this version posted March 5, 2021. The copyright holder for this preprint (which was not certified by peer review) is the author/funder. All rights reserved. No reuse allowed without permission.

274 longer positioning Ser23 and Lys45 to hydrogen bond with the phosphates of T_{-7} and T_{-4}
275 (**Fig. 5B; Fig. S3**).

276 Global comparison of the $HigB_2HigA_2$-O2 structure with the $HigBHigA_2$-O2 structure
277 reveal only a ~1° difference emphasizing how similar the two structures are (**Fig. 5D**).
278 Likewise there are very little differences in the position of $HigA_2$ bound to O2 (38) in the
279 absence or presence of HigB. Thus, it does not appear that HigB binding influences the
280 position of $HigA_2$ on DNA. It appears the largest structural change results from either $HigA_2$
281 or $HigB_nHigA_2$ binding to DNA (~14° rotation, where "n" denotes either a single HigB or two
282 HigB monomers; **Fig. 4D**). Previously we described how HigA N-terminal residues Arg2 and
283 Gln3 interact with its C-terminal residues Arg77 and Glu80 in the $HigB_2HigA_2$-O2 structure
284 (**Fig. 4C**). We find that even a single HigB binding can cause these termini residues to
285 become ordered (**Fig. S4E**).

286 A curious crystallization note for the trimeric $HigBHigA_2$-O2 complex is that there is
287 an adjacent molecule in the neighboring asymmetric unit that overlaps with the missing HigB
288 (**Fig. S6**). This ejection of HigB from the HigBHigA complex is surprising given the known
289 tight interactions of TA complexes where affinities are typically sub-nanomolar (29, 40-42).
290 Therefore, we think it is unlikely that the trimeric $HigBHigA_2$-O2 complex results from crystal
291 packing. Interestingly, the structures of both HigBHigA complexes with the different
292 placement of the His_6 tag were solved and both found to be tetrameric $HigB_2HigA_2$ in the
293 absence of DNA. Taken together, we propose that there is a mixture of both trimeric and
294 tetrameric HigBHigA complexes bound to DNA in solution. We next sought to examine the
295 functional relevance of the trimeric $HigBHigA_2$-O2 complex.

296

297 **$HigB_2A_2$-O2 and $HigBHigA_2$-O2 complexes exhibit similar dynamics.** The structure of
298 the trimeric $HigBHigA_2$-O2 complex is intriguing as most models that describe the

bioRxiv preprint doi: https://doi.org/10.1101/2021.03.04.434028; this version posted March 5, 2021. The copyright holder for this preprint (which was not certified by peer review) is the author/funder. All rights reserved. No reuse allowed without permission.

299 transcriptional regulation of type II TA systems conclude that such an oligomeric state is
300 more stable than the fully loaded complex (18, 21, 42). However, prior to our new structure,
301 there has been no biochemical or direct evidence for the existence of this oligomeric state.
302 To assess the dynamics of both complexes in the presence or absence of O2, we performed
303 molecular dynamics (MD) simulations of four complexes: $HigB_2HigA_2$ and $HigBHigA_2$ in the
304 presence or absence of O2 (**Fig. 6**). The trimeric $HigBHigA_2$ complex in the absence of DNA
305 has not been solved and we generated the model based upon the $HigBHigA_2$-O2 structure.
306 We obtained 1 microsecond-long MD trajectories of each complex and subsequently
307 performed root mean square fluctuation (RMSF) analysis. This analysis reveals overall
308 comparable dynamics: in tetrameric $HigB_2HigA_2$, binding to O2 only marginally affects
309 dynamics, with the largest effects observed at intrinsically flexible regions such as the C
310 termini of HigA monomers (residues 94-102) and loop 3 of HigB (residues 56-62) (**Fig. 6A**).
311 In trimeric $HigBHigA_2$, similar trends are observed, confirming that both oligomeric states
312 represent similarly stable, DNA-bound complexes (**Fig. 6B**). One noted difference is that in
313 the trimeric $HigBHigA_2$-O2 complex, the C-termini of one of the two HigAs is disordered and
314 is not modeled. Two HigB monomers binding causes the C-termini of HigA to regain order
315 but while the C-termini of both HigA monomers can be modeled, this region still exhibits
316 dynamic behavior.
317
318 **Engineered trimeric $HigBHigA_2$ transcriptionally represses P*hig*.** To test whether a
319 trimeric $HigBHigA_2$ complex represses transcription to the same extent as $HigB_2HigA_2$, we
320 attempted to engineer such a variant. Comparison of the $HigB_2HigA_2$ structure with the
321 $HigB_2HigA_2$-O2 DNA structure shows that the two HigB monomers move closer to each other
322 to accommodate binding to DNA (**Fig. 7A**). In particular, HigB loop 5 (L5) located at the
323 interface of the HigB monomers moves ~4Å (**Fig. 4D**). We therefore extended L5 by the

bioRxiv preprint doi: https://doi.org/10.1101/2021.03.04.434028; this version posted March 5, 2021. The copyright holder for this preprint (which was not certified by peer review) is the author/funder. All rights reserved. No reuse allowed without permission.

324 addition of a short, flexible sequence of four residues (Asn, Gly, Asn, Gly (NGNG); called
325 HigB(L5ext)HigA$_2$) to prevent concurrent binding of two HigB monomers to HigA$_2$ (**Fig. 7A**).
326 Expression and purification of HigB(L5ext)HigA$_2$ showed a delayed elution of the complex
327 from the size exclusion column as compared to wild-type HigB$_2$HigA$_2$ (**Fig. 7B**), at a volume
328 corresponding to a molecular weight of 42 kDa (compared to 56 kDa for wild-type
329 HigB$_2$HigA$_2$). The difference in apparent molecular weights indicates that the
330 HigB(L5ext)HigA$_2$ complex is ~14 kDa smaller than the wild-type complex which roughly
331 corresponds to a HigB monomer (molecular weight of ~13 kDa). To assess its thermal
332 stability, we performed nano-differential scanning fluorimetry (nano-DSF) which provides
333 information on the melting temperature (T_m) of the complex. Since this measurement is not
334 at equilibrium, the inflection point is known as T_i. HigB(L5ext)HigA$_2$ is ~5ºC less thermostable
335 than wild-type HigB$_2$HigA$_2$ (60.5ºC vs. 54.0ºC) consistent with an altered oligomeric state
336 (**Fig. 7C**).

337 To test the ability of the HigB(L5ext)HigA$_2$ variant to repress transcription at *hig*, we
338 performed EMSA and β-gal assays using similar approaches as described above. The
339 HigB(L5ext)HigA$_2$ complex binds to both O1 and O2 DNAs at concentrations similar to wild-
340 type HigB$_2$HigA$_2$ (**Fig. 8A**). Although an intermediate shift is observed (likely representing a
341 HigA$_2$ dimer bound), these data show the trimeric HigB(L5ext)HigA$_2$ interacts with O1 and
342 O2 in a similar manner as wild-type HigB$_2$HigA$_2$. To determine whether the HigB(L5ext)HigA$_2$
343 complex represses P*hig in vivo*, we used the previously described P*hig* constructs and
344 included a P*hig* containing the HigB(L5ext)HigA$_2$ variant (pQF50-P*hig*-*higB*(L5ext)*higA*-*lacZ*;
345 **Fig. 8B; Fig. S7**). As expected, P*hig* alone shows high β-gal activity (normalize to 0%
346 repression) because of the absence of transcriptional repressor HigA. P*hig*-*higBhigA*-*lacZ*
347 shows little β-gal activity indicating robust HigA repression at P*hig* (~95% repression). The

bioRxiv preprint doi: https://doi.org/10.1101/2021.03.04.434028; this version posted March 5, 2021. The copyright holder for this preprint (which was not certified by peer review) is the author/funder. All rights reserved. No reuse allowed without permission.

348 HigB(L5ext)HigA$_2$ variant shows similar repression as wild-type HigB$_2$HigA$_2$ suggesting
349 there is no difference between a trimeric or tetrameric HigBHigA complex.

350 One possibility that we wanted to explore was whether *hig* is responsive to changing
351 toxin levels *in vivo* considering that toxin overexpression in the *phddoc*, *ccdBccdA* and *relEB*
352 systems can relieve repression (17, 18, 27). For this assay, we used a HigB variant (H54A)
353 that is not catalytically active so cell growth won't be impacted by its expression and we
354 know this variant is expressed as detected by Western blot analysis (34, 43). Further, since
355 the active site of HigB is on the opposite surface from its HigA binding surface (26), this
356 variant should not interfere with HigA binding. Overexpression of HigB(H54A) showed
357 minimal impact on repression of P*hig-higBhigA* indicating free HigB(H54A) is unable to
358 interact with HigB$_2$HigA$_2$ bound at O1 or O2 (97.2% vs. 98.0%; **Fig. 8B**). In the case of the
359 engineered HigB(L5ext)HigA$_2$, excess HigB(H54A) expression also has no effect on
360 repression and does not interfere with HigA-mediated repression (**Fig. 8B**). These data
361 support a model whereby *hig* repression is only relieved by HigA proteolysis.

362

363 **DISCUSSION**

364 The roles of bacterial TA modules have been controversial owing to experimental errors in
365 the construction of *E. coli* TA deletion strains and the ambiguity over what activates toxin
366 expression, antitoxin proteolysis and the release of toxin (10, 44, 45). While these activities
367 are still under debate, the way these modules are transcriptionally autoregulated is known
368 to clearly contribute to their changing expression patterns in response to external stimuli
369 although many outstanding questions still remain (17, 18, 27). One question is how different
370 oligomeric TA complexes influence physical interactions with their DNA operators and the
371 assembly and/ or cooperativity of TA complexes bound at adjacent operator sites. In this
372 study, we focused on the regulation of the *higBhigA* TA module first identified on the

bioRxiv preprint doi: https://doi.org/10.1101/2021.03.04.434028; this version posted March 5, 2021. The copyright holder for this preprint (which was not certified by peer review) is the author/funder. All rights reserved. No reuse allowed without permission.

373 antibiotic-resistance Rts1 plasmid associated with a urinary tract infection caused by *P.*
374 *vulgaris* (32). Our prior work revealed that while the HigB toxin adopts a canonical
375 ribonuclease fold similar to other members of the RelE family (26), HigA antitoxin suppresses
376 HigB activity in an unusual manner, suggesting that transcriptional repression may also be
377 different. We therefore sought to understand how the *higBhigA* operon is regulated and how
378 its diverse architecture might influence its negative regulation of transcription.

379 Higher-order oligomeric complexes of the PhDDoc, RelBRelE and CcdBCcdA TA
380 complexes alter their thermodynamic interactions with operators and thus influence
381 transcriptional responsiveness (17, 18, 27). We find that although HigA binding at adjacent
382 operators is not cooperative (38) (**Fig. 2**), the addition of HigB promotes the formation of
383 higher-order complexes and disassembly of the complex does appear to occur once a
384 threshold of excess toxin to antitoxin is reached (**Figs. 2,3**). On the surface, these data
385 appear to be consistent with how other TAs are regulated via the conditional cooperativity
386 model or, as other transcriptional systems are described, as molecular rheostats (14).
387 However, in an attempt to perturb the system *in vivo* by increasing HigB concentrations in
388 the presence of the HigBHigA complex bound at O1 and O2 operators, we find no observable
389 change in repression in contrast to these TA systems (**Fig. 8B**). These conflicting data
390 indicate that the perceived disruption of the higher order HigBHigA-O2 DNA complex via
391 EMSA may not be reflective of transcriptional repression that we observe *in vivo*. Further,
392 these results suggest a different mode of regulation for the *higBhigA* operon.

393 One hallmark of conditional cooperativity that defines transcriptional regulation of TA
394 operons is that the addition of excess toxin to antitoxins bound at operator sites changes the
395 affinity of these interactions because toxin can act both as a co-repressor and de-repressor
396 (17, 18, 22). In general, when the toxin and antitoxin are expressed at equimolar ratios, the
397 toxin functions as a co-repressor and transcriptional repression is enhanced. Once toxin

bioRxiv preprint doi: https://doi.org/10.1101/2021.03.04.434028; this version posted March 5, 2021. The copyright holder for this preprint (which was not certified by peer review) is the author/funder. All rights reserved. No reuse allowed without permission.

398 concentrations exceed that of the antitoxin, however, disruption of the repressor complex
399 ensues, antitoxin disengages from the promoter, and transcription proceeds (**Fig. 1**). To
400 achieve this mode of regulation, defined oligomeric states of TA complexes have different
401 affinities: for example, although the structure of RelBRelE complex indicates the complex is
402 tetrameric with two RelE toxins and two RelB antitoxins (21), a trimeric version of the
403 complex (two RelBs, one RelE) is proposed to have the highest affinity for the *rel* operon
404 (18, 21). In the presence of a greater excess of toxin, the tetrameric $RelB_2RelE_2$ forms at
405 adjacent operators causing a change from a high affinity to a low affinity state, and the
406 RelBRelE complex no longer binds to DNA (**Fig. 1**). This model permits the system to be
407 responsive to changing levels of toxin but at this point, there is limited biochemical and
408 structural data that corresponds to these changing oligomeric states.

409 We serendipitously solved two different structures of the HigBHigA-O2 complexes
410 that differ in their molar ratios of HigA antitoxin to the HigB toxin (**Figs. 4,5**). These different
411 oligomeric states capture, for the first time, how both the tetrameric $HigB_2HigA_2$ and trimeric
412 $HigBHigA_2$ interact with O2 to repress transcription. The trimeric $HigBHigA_2$-O2 DNA
413 structure was especially unexpected given that the tetrameric $HigB_2HigA_2$ form predominates
414 in the absence of operator (26). The molecular interactions of each HigBHigA complex with
415 its operator are largely maintained, initially suggesting that different oligomeric states may
416 not contribute to changes in repression for this system. Molecular dynamic simulations of
417 both the trimeric and tetrameric HigBHigA-O2 complexes show each complex have similar
418 dynamics when bound to DNA, offering further support for the ability of both oligomeric states
419 to contribute to repression (**Fig. 6**). Further, engineering of a forced trimeric $HigBHigA_2$
420 oligomeric complex revealed similar levels of transcriptional repression (**Figs. 7,8; Fig. S7**).
421 Together, these data support a model where *hig* is regulated as a simple on/off switch

bioRxiv preprint doi: https://doi.org/10.1101/2021.03.04.434028; this version posted March 5, 2021. The copyright holder for this preprint (which was not certified by peer review) is the author/funder. All rights reserved. No reuse allowed without permission.

422 incalcitrant to changing levels of toxin and influenced solely by HigA proteolysis likely as
423 result of the Rts1 plasmid not being inherited.

424 There are several other reasons for why *hig* may be regulated in a different manner
425 from other TA operons. In TA operons regulated as molecular rheostats including *phddoc*,
426 *relBrelE* and *ccdBccdA*, a single promoter controls expression of the operon and the
427 antitoxin is encoded first (17, 18, 22). It has been suggested this operon organization allows
428 for the antitoxin to be expressed in excess of the toxin, which is required to suppress toxicity
429 when the system is transcriptionally de-repressed (46, 47). In *hig*, there is a second weak
430 promoter, P*higA*, that allows for independent expression of HigA to ensure excess HigA is
431 always present to suppress HigB (48). It is not clear if this change in operon organization
432 accounts for why *hig* is regulated via a simple on/off switch but other TA operons such as
433 *mqsRA* that also have this reverse architecture and contain multiple promoters do not appear
434 to be regulated via conditional cooperativity (29). In contrast, the DinJ-YafQ TA module does
435 not have this reverse architecture but does not appear to be regulated by conditional
436 cooperativity (30). Therefore, there must be some other currently unappreciated mechanism
437 by which this TA system balances antitoxin expression for its regulation.

438 The results presented here provide new insight into the transcriptional regulation of
439 the plasmid-associated *hig* operon and add to the growing diversity of mechanisms used to
440 balance transcriptional responses of these abundant bacterial gene pairs. In the future,
441 additional biophysical studies are needed to reconcile the role of changing macromolecular
442 complex formation in the regulation of TA pairs and to align these properties with
443 transcriptional responsiveness.

444

445 **MATERIALS AND METHODS**

bioRxiv preprint doi: https://doi.org/10.1101/2021.03.04.434028; this version posted March 5, 2021. The copyright holder for this preprint (which was not certified by peer review) is the author/funder. All rights reserved. No reuse allowed without permission.

446 **Strains and plasmids**. *E. coli* BL21(DE3) cells were used for expression of His_6-HigA, His_6-
447 HigBHigA and HigBHigA-His_6 proteins from pET28a, pET28a and pET21c vectors,
448 respectively as previously reported (26). *E. coli* BW25113 cells were used for all β-gal
449 experiments and HigB(H54A)-His_6 expression (49). All point mutations were introduced by
450 site-directed mutagenesis and sequences were verified by DNA sequencing (Genewiz).
451

452 **HigA, HigB and HigBHigA expression and purification.** The His_6-HigA, His_6-HigBHigA
453 and HigBHigA-His_6 protein complexes were overexpressed and purified as previously
454 described with minor modifications (26). These differences included incubation of His_6-HigA
455 at 18°C overnight after protein induction and removal of the His_6 tag from His_6-HigA and His_6-
456 HigBHigA with thrombin prior to gel filtration chromatography. HigB(H54A) protein was
457 overexpressed and purified as previously described (43).
458

459 **Electrophoretic mobility shift assays (EMSAs).** To construct the dsDNA for the EMSA,
460 pairs of complementary single-stranded oligonucleotides were diluted to 2 µM each in 100
461 mM NaCl, 10 mM Tris-HCl pH8. The O1-O2, O1-O2(scrambled) or O1(scrambled)-O2
462 oligonucleotide mixtures (**Table S1**) of the *hig* promoter fragment were incubated in boiling
463 water and then cooled at room temperature overnight. The dsDNA oligos were diluted to 150
464 nM in EMSA binding buffer (100 mM NaCl, 10 mM $MgCl_2$, 5% glycerol, 0.01 mg/mL bovine
465 serum albumin). Purified wild-type HigA, HigBHigA, and HigB(L5ext)HigA proteins were
466 diluted to 10 µM in EMSA binding buffer and serially diluted to give a series of protein
467 concentrations ranging from 25 nM to 0.8 µM. The binding reactions were incubated on ice
468 for 20 min and 10 µL of each reaction was loaded onto 8% native, polyacrylamide-0.5X
469 TBE/10% glycerol gels (50 mM Tris-HCl pH 8, 50 mM boric acid, 5 mM EDTA, 10% glycerol)
470 and subjected to electrophoresis at 110 V limiting on ice for 60 min. To visualize the DNA

bioRxiv preprint doi: https://doi.org/10.1101/2021.03.04.434028; this version posted March 5, 2021. The copyright holder for this preprint (which was not certified by peer review) is the author/funder. All rights reserved. No reuse allowed without permission.

471 and DNA-protein complexes, the gels were stained with SYBR green nucleic acid gel stain
472 (ThermoFisher Scientific) in 0.5X TBE/10% glycerol for 30 min with gentle agitation and then
473 the fluorescence was imaged with a Typhoon Trio phosphoimager (GE Healthcare; 488 nm
474 excitation and 526 nm emission). Assays were performed in duplicate with representative
475 gels shown. Band intensities for both free and bound *hig* DNA were quantified with
476 ImageQuant 1D gel analysis software using the rolling ball background subtraction. For HigA
477 or HigBHigA bound to either O1 or O2, the binding data were fit using a one site-specific
478 binding equation (Y (specific binding , μM) = Bmax * X / [K_D + X]) in GraphPad Prism 9.0.0.
479

480 **Crystallization, data collection and structure determination of the HigBHigA-O2 DNA**
481 **complexes.** The complex was formed by mixing either His_6-HigBHigA or selenomethionine-
482 derivatized HigBHigA-His_6 (both in 40 mM Tris-HCl, pH 7.5, 250 mM KCl, 5 mM $MgCl_2$, and
483 5 mM β-mercaptoethanol) with O2 operator DNA (10 mM Tris, pH 8, 100 mM NaCl, and 1
484 mM EDTA) at one $HigB_2HigA_2$ tetramer to one O2 dsDNA molar ratio. The complexes were
485 diluted to 5.95 mg/mL HigBHigA and 1.55 mg/mL O2 DNA by the addition of buffer (20 mM
486 Tris, pH 8, 10 mM $MgCl_2$, and 100 mM NaCl). Crystals of HigBHigA bound to O2 DNA were
487 grown by sitting drop vapor diffusion and crystallized in 0.2 M $CaCl_2$ and 10-25% (w/v)
488 polyethylene glycol 3,350 at 20°C. Both crystal forms grew after two days and were
489 cryoprotected by serially increasing the concentration of ethylene glycol in the mother liquor
490 from 10-30% (w/v) followed by flash freezing in liquid nitrogen.

491 Two X-ray datasets were collected at the Northeastern Collaborative Access Team
492 (NE-CAT) 24-ID-C and Southeast Regional Collaborative Access Team (SER-CAT) 22-ID
493 facilities at the Advanced Photon Source (APS) at the Argonne National Laboratory. For the
494 tetrameric $HigB_2HigA_2$-O2 complex, 360° of data (0.5° oscillations) were collected on a
495 PILATUS 6M-F detector (DECTRIS Ltd., Switzerland) using 0.9792 Å radiation. For the

bioRxiv preprint doi: https://doi.org/10.1101/2021.03.04.434028; this version posted March 5, 2021. The copyright holder for this preprint (which was not certified by peer review) is the author/funder. All rights reserved. No reuse allowed without permission.

496 trimeric HigBHigA$_2$-O2 complex, 90° of data (0.5° oscillations) were collected on a
497 MARMOSAIC 300 mm CCD detector (Rayonix, L.L.C., USA) using 1.0 Å radiation. XDS was
498 used to integrate and scale the data (50). The tetrameric HigB$_2$HigA$_2$-O2 structure was
499 solved by single wavelength anomalous diffraction phasing using AutoSol from the PHENIX
500 software suite (51) and thirteen heavy atom sites were found. The trimeric HigBHigA$_2$-O2
501 structure was solved using the structure of the HigA$_2$ dimer (PDB code 6CF1) as a molecular
502 replacement search model in the PHENIX software suite. XYZ coordinates, real space, and
503 B-factors (isotropic) were refined iteratively in PHENIX and model building was performed
504 using the program Coot (52). Final refinement of the structures gave crystallographic
505 R_{work}/R_{free} of 17.6/21.8% for trimeric HigBHigA$_2$-O2 and 17.5/22.1% for tetrameric
506 HigB$_2$HigA$_2$-O2. All figures were created in PyMol (53).
507
508 **β-galactosidase assays.** The *hig* operon was chemically synthesized (IDT), digested and
509 ligated into a pQF50 vector with *lacZ* downstream (pQF50-*hig* constructs). *E. coli* BW25113
510 transformed with pQF50-*hig* variants or pBAD33-*higB*(H54A) were used for all experiments.
511 Two methods were used to perform β-gal assays. The first set of β-gal assays presented
512 herein (with constructs containing wild-type versus mutated operators) were performed using
513 the PopCulture® Reagent based method (54). All overnight cultures were grown in M9
514 minimal media supplemented with 0.2% glucose, 1 M $MgSO_4$, 1 M $CaCl_2$, and 10% casamino
515 acids. Subsequent experiments were performed with M9 minimal media supplemented with
516 20% glycerol instead of glucose. OD_{600} was measured hourly until an OD_{600} of 0.2 was
517 reached, arabinose was added to a final concentration of 0.2%, and further incubated for 4
518 hrs. 1 mL aliquots were pelleted, resuspended in 500 µL of M9 media and diluted to an OD_{600}
519 of 0.5 in M9 media. 80 µL were transferred to 96-well plate and 120 µL of freshly mixed β-
520 gal reagent (60 mM Na_2SO_4, 40 mM NaH_2PO_4, 10 mM KCl, 1 mM $MgSO_4$, 36 mM β-me, 166

bioRxiv preprint doi: https://doi.org/10.1101/2021.03.04.434028; this version posted March 5, 2021. The copyright holder for this preprint (which was not certified by peer review) is the author/funder. All rights reserved. No reuse allowed without permission.

521 μL/mL T7 lysozyme, 1.1 mg/mL ortho-Nitrophenyl-β-galactoside and 6.7% PopCulture®
522 Reagent (Millipore-Sigma)) was added to each well. 80 μL of M9 media was also added to
523 wells containing 120 μL of β-gal reagent as a negative control. The microplate was read by
524 a Biotek Cytation 5 multi-mode reader pre-incubated at 30°C, with OD_{600} and OD_{420}
525 measurements taken every 5 min for 1 hr with agitation.

526 The second set of β-gal assays presented herein (in the absence or presence of
527 HigB(H54A)) were performed using a method previously described (38). In both approaches,
528 activity in Miller Units (M.U.) was measured using the formula: total activity (M.U.) =
529 $(1000*OD_{420})$ / $(OD_{600}$ * volume of culture used (mL) * 0.5). Assays were performed in
530 triplicate with two technical replicates.

531

532 **Differential scanning fluorimetry (DSF).** The thermal stability of wild-type HigBHigA and
533 HigB(L5ext)HigA were assessed using a Tycho NT.6 instrument (NanoTemper). Protein was
534 heated at 0.1ºC steps over a temperature range of 35ºC to 95ºC, during which intrinsic
535 fluorescence at 350 and 330 nm was measured. Inflection temperature (T_i) was determined
536 for each apparent unfolding transition from the temperature-dependent change in the ratio
537 of 350 and 330 nm measurements. Assays were performed in triplicates.

538

539 **Molecular dynamics simulations.** Starting models for molecular dynamics (MD)
540 simulations were prepared from PDB codes 6W6U ($HigB_2HigA_2$-O2) and 6WFP ($HigBHigA_2$-
541 O2). Simulations were performed on the tetrameric or trimeric HigBHigA structures in the
542 absence or presence of O2 DNA ($HigB_2HigA_2$-O2, $HigBHigA_2$-O2, $HigB_2HigA_2$ and
543 $HigBHigA_2$). All complexes were prepared using the Xleap module of AmberTools 18 (55),
544 the ff14SB forcefield for protein atoms (56) and the OL15 forcefield (57) for DNA. Complexes
545 were solvated in an octahedral box of TIP3P water (58) with a 10 Å buffer. Ions were added

bioRxiv preprint doi: https://doi.org/10.1101/2021.03.04.434028; this version posted March 5, 2021. The copyright holder for this preprint (which was not certified by peer review) is the author/funder. All rights reserved. No reuse allowed without permission.

546 to each complex to achieve a final concentration of 150 mM NaCl. Minimization was
547 performed in three rounds, each employing steepest descent (5000 steps) followed by
548 conjugate gradient (5000 steps). In the first round, restraints of 500 kcal/mol-Å^2 were applied
549 to all solute atoms. In the second round, solute restraints were reduced to 100 kcal/mol-Å^2.
550 All restraints were removed in the third round. Complexes were heated from 0 to 300 K with
551 a 100-ps run with constant volume periodic boundaries and restraints of 10-kcal/mol-Å^2 on
552 solute atoms. All MD simulations were performed using AMBER2018 (55, 59, 60). Two
553 stages of equilibration were performed: 10 ns MD in the NPT ensemble with 10-kcal/mol-Å^2
554 restraints on solute atoms, followed by an additional 10 ns MD run with restraints reduced
555 to 1 kcal/mol-Å^2. Finally all restraints were removed and 1 microsecond production
556 simulations obtained for each complex. Long-range electrostatics were evaluated with a
557 cutoff of 10 Å and all heavy atom-hydrogen bonds were fixed with the SHAKE algorithm (61).
558 Following MD, the CPPTRAJ module (62) of AmberTools 18 was used to calculate root mean
559 square fluctuations (RMSF) of each protein reside in each complex.
560

561 **ACKNOWLEDGEMENTS**

562 Research reported in this publication was partially supported by a National Science
563 Foundation CAREER award MCB 0953714 (CMD), a NIH Biochemistry, Cellular and
564 Molecular Biology Graduate Training Grant 5T32GM8367 (MAS), and NIH NRSA F31
565 Fellowship GM108351 (MAS) and a Burroughs Wellcome Fund Investigator in the
566 Pathogenesis of Infectious Disease award (CMD). We thank F. M. Murphy IV and staff
567 members of the NE-CAT beamlines for assistance during data collection and G. L. Conn
568 and other Dunham lab members for critical reading of the manuscript. This work is based
569 upon research conducted at the Northeastern Collaborative Access Team beamlines, which
570 are funded by the National Institute of General Medical Sciences from the National Institutes

bioRxiv preprint doi: https://doi.org/10.1101/2021.03.04.434028; this version posted March 5, 2021. The copyright holder for this preprint (which was not certified by peer review) is the author/funder. All rights reserved. No reuse allowed without permission.

of Health (P30 GM124165). Additional data were collected at the Southeast Regional Collaborative Access Team (SER-CAT) 22-ID (or 22-BM) beamline at the Advanced Photon Source, Argonne National Laboratory. SER-CAT is supported by its member institutions (www.ser-cat.org/members.html) and equipment grants (S10RR25528 and S10RR028976) from the National Institutes of Health. Use of the Advanced Photon Source was supported by the U. S. Department of Energy, Office of Science, Office of Basic Energy Sciences, under Contract No. DE-AC02-06CH11357.

REFERENCES

1. D. P. Pandey, K. Gerdes, Toxin-antitoxin loci are highly abundant in free-living but lost from host-associated prokaryotes. *Nucleic Acids Res* **33**, 966-976 (2005).
2. K. S. Makarova, Y. I. Wolf, E. V. Koonin, Comprehensive comparative-genomic analysis of type 2 toxin-antitoxin systems and related mobile stress response systems in prokaryotes. *Biol Direct* **4**, 19 (2009).
3. R. Leplae *et al.*, Diversity of bacterial type II toxin-antitoxin systems: a comprehensive search and functional analysis of novel families. *Nucleic Acids Res* **39**, 5513-5525 (2011).
4. H. Karoui, F. Bex, P. Dreze, M. Couturier, Ham22, a mini-F mutation which is lethal to host cell and promotes recA-dependent induction of lambdoid prophage. *EMBO J* **2**, 1863-1868 (1983).
5. T. Ogura, S. Hiraga, Mini-F plasmid genes that couple host cell division to plasmid proliferation. *Proc Natl Acad Sci U S A* **80**, 4784-4788 (1983).
6. K. Gerdes, P. B. Rasmussen, S. Molin, Unique type of plasmid maintenance function: postsegregational killing of plasmid-free cells. *Proc Natl Acad Sci U S A* **83**, 3116-3120 (1986).

bioRxiv preprint doi: https://doi.org/10.1101/2021.03.04.434028; this version posted March 5, 2021. The copyright holder for this preprint (which was not certified by peer review) is the author/funder. All rights reserved. No reuse allowed without permission.

595 7. A. Bravo, G. de Torrontegui, R. Diaz, Identification of components of a new stability system
596 of plasmid R1, ParD, that is close to the origin of replication of this plasmid. *Mol Gen Genet*
597 **210**, 101-110 (1987).
598 8. S. Tsuchimoto, H. Ohtsubo, E. Ohtsubo, Two genes, pemK and pemI, responsible for stable
599 maintenance of resistance plasmid R100. *J Bacteriol* **170**, 1461-1466 (1988).
600 9. H. Lehnherr, E. Maguin, S. Jafri, M. B. Yarmolinsky, Plasmid addiction genes of
601 bacteriophage P1: doc, which causes cell death on curing of prophage, and phd, which
602 prevents host death when prophage is retained. *Journal of molecular biology* **233**, 414-428
603 (1993).
604 10. N. Fraikin, F. Goormaghtigh, L. Van Melderen, Type II Toxin-Antitoxin Systems: Evolution
605 and Revolutions. *J Bacteriol* **202** (2020).
606 11. R. Loris, A. Garcia-Pino, Disorder- and dynamics-based regulatory mechanisms in toxin-
607 antitoxin modules. *Chemical reviews* **114**, 6933-6947 (2014).
608 12. R. Page, W. Peti, Toxin-antitoxin systems in bacterial growth arrest and persistence. *Nat*
609 *Chem Biol* **12**, 208-214 (2016).
610 13. F. M. Rossi, A. M. Kringstein, A. Spicher, O. M. Guicherit, H. M. Blau, Transcriptional control:
611 rheostat converted to on/off switch. *Mol Cell* **6**, 723-728 (2000).
612 14. E. Batchelor, T. J. Silhavy, M. Goulian, Continuous control in bacterial regulatory circuits. *J*
613 *Bacteriol* **186**, 7618-7625 (2004).
614 15. M. Gotfredsen, K. Gerdes, The Escherichia coli relBE genes belong to a new toxin-antitoxin
615 gene family. *Mol Microbiol* **29**, 1065-1076 (1998).
616 16. R. Magnuson, M. B. Yarmolinsky, Corepression of the P1 addiction operon by Phd and Doc.
617 *J Bacteriol* **180**, 6342-6351 (1998).
618 17. H. Afif, N. Allali, M. Couturier, L. Van Melderen, The ratio between CcdA and CcdB modulates
619 the transcriptional repression of the ccd poison-antidote system. *Mol Microbiol* **41**, 73-82
620 (2001).

bioRxiv preprint doi: https://doi.org/10.1101/2021.03.04.434028; this version posted March 5, 2021. The copyright holder for this preprint (which was not certified by peer review) is the author/funder. All rights reserved. No reuse allowed without permission.

621 18. M. Overgaard, J. Borch, M. G. Jorgensen, K. Gerdes, Messenger RNA interferase RelE
622 controls relBE transcription by conditional cooperativity. *Mol Microbiol* **69**, 841-857 (2008).
623 19. A. Harms, D. E. Brodersen, N. Mitarai, K. Gerdes, Toxins, Targets, and Triggers: An Overview
624 of Toxin-Antitoxin Biology. *Mol Cell* **70**, 768-784 (2018).
625 20. T. Madl *et al.*, Structural basis for nucleic acid and toxin recognition of the bacterial antitoxin
626 CcdA. *Journal of molecular biology* **364**, 170-185 (2006).
627 21. A. Boggild *et al.*, The crystal structure of the intact E. coli RelBE toxin-antitoxin complex
628 provides the structural basis for conditional cooperativity. *Structure* **20**, 1641-1648 (2012).
629 22. A. Garcia-Pino *et al.*, Allostery and intrinsic disorder mediate transcription regulation by
630 conditional cooperativity. *Cell* **142**, 101-111 (2010).
631 23. C. Dienemann, A. Boggild, K. S. Winther, K. Gerdes, D. E. Brodersen, Crystal structure of
632 the VapBC toxin-antitoxin complex from Shigella flexneri reveals a hetero-octameric DNA-
633 binding assembly. *Journal of molecular biology* **414**, 713-722 (2011).
634 24. B. L. Brown *et al.*, Three dimensional structure of the MqsR:MqsA complex: a novel TA pair
635 comprised of a toxin homologous to RelE and an antitoxin with unique properties. *PLoS*
636 *Pathog* **5**, e1000706 (2009).
637 25. M. A. Schumacher *et al.*, Molecular mechanisms of HipA-mediated multidrug tolerance and
638 its neutralization by HipB. *Science* **323**, 396-401 (2009).
639 26. M. A. Schureck *et al.*, Structure of the Proteus vulgaris HigB-(HigA)2-HigB toxin-antitoxin
640 complex. *J Biol Chem* **289**, 1060-1070 (2014).
641 27. R. Magnuson, H. Lehnherr, G. Mukhopadhyay, M. B. Yarmolinsky, Autoregulation of the
642 plasmid addiction operon of bacteriophage P1. *J Biol Chem* **271**, 18705-18710 (1996).
643 28. I. Brzozowska, U. Zielenkiewicz, Regulation of toxin-antitoxin systems by proteolysis. *Plasmid*
644 **70**, 33-41 (2013).
645 29. B. L. Brown, D. M. Lord, S. Grigoriu, W. Peti, R. Page, The Escherichia coli toxin MqsR
646 destabilizes the transcriptional repression complex formed between the antitoxin MqsA and
647 the mqsRA operon promoter. *J Biol Chem* **288**, 1286-1294 (2013).

bioRxiv preprint doi: https://doi.org/10.1101/2021.03.04.434028; this version posted March 5, 2021. The copyright holder for this preprint (which was not certified by peer review) is the author/funder. All rights reserved. No reuse allowed without permission.

648 30. A. Ruangprasert *et al.*, Mechanisms of toxin inhibition and transcriptional repression by
649 Escherichia coli DinJ-YafQ. *J Biol Chem* **289**, 20559-20569 (2014).
650 31. Y. Terawaki, H. Takayasu, T. Akiba, Thermosensitive replication of a kanamycin resistance
651 factor. *J Bacteriol* **94**, 687-690 (1967).
652 32. Q. B. Tian, M. Ohnishi, A. Tabuchi, Y. Terawaki, A new plasmid-encoded proteic killer gene
653 system: cloning, sequencing, and analyzing hig locus of plasmid Rts1. *Biochem Biophys Res*
654 *Commun* **220**, 280-284 (1996).
655 33. J. M. Hurley, N. A. Woychik, Bacterial toxin HigB associates with ribosomes and mediates
656 translation-dependent mRNA cleavage at A-rich sites. *J Biol Chem* **284**, 18605-18613 (2009).
657 34. M. A. Schureck, J. A. Dunkle, T. Maehigashi, S. J. Miles, C. M. Dunham, Defining the mRNA
658 recognition signature of a bacterial toxin protein. *Proc Natl Acad Sci U S A* **112**, 13862-13867
659 (2015).
660 35. M. A. Schureck, T. Maehigashi, S. J. Miles, J. Marquez, C. M. Dunham, mRNA bound to the
661 30S subunit is a HigB toxin substrate. *RNA* **22**, 1261-1270 (2016).
662 36. S. Hadzi *et al.*, Ribosome-dependent Vibrio cholerae mRNAse HigB2 is regulated by a beta-
663 strand sliding mechanism. *Nucleic Acids Res* **45**, 4972-4983 (2017).
664 37. B. S. Xu *et al.*, Conformational changes of antitoxin HigA from Escherichia coli str. K-12 upon
665 binding of its cognate toxin HigB reveal a new regulation mechanism in toxin-antitoxin
666 systems. *Biochem Biophys Res Commun* **514**, 37-43 (2019).
667 38. M. A. Schureck *et al.*, Structural basis of transcriptional regulation by the HigA antitoxin. *Mol*
668 *Microbiol* **111**, 1449-1462 (2019).
669 39. Q. B. Tian *et al.*, Specific protein-DNA and protein-protein interaction in the hig gene system,
670 a plasmid-borne proteic killer gene system of plasmid Rts1. *Plasmid* **45**, 63-74 (2001).
671 40. M. H. Dao-Thi *et al.*, Molecular basis of gyrase poisoning by the addiction toxin CcdB. *Journal*
672 *of molecular biology* **348**, 1091-1102 (2005).

bioRxiv preprint doi: https://doi.org/10.1101/2021.03.04.434028; this version posted March 5, 2021. The copyright holder for this preprint (which was not certified by peer review) is the author/funder. All rights reserved. No reuse allowed without permission.

673 41. S. K. Khoo *et al.*, Molecular and structural characterization of the PezAT chromosomal toxin-
674 antitoxin system of the human pathogen Streptococcus pneumoniae. *J Biol Chem* **282**,
675 19606-19618 (2007).
676 42. M. Overgaard, J. Borch, K. Gerdes, RelB and RelE of Escherichia coli form a tight complex
677 that represses transcription via the ribbon-helix-helix motif in RelB. *Journal of molecular*
678 *biology* **394**, 183-196 (2009).
679 43. M. A. Schureck, A. Repack, S. J. Miles, J. Marquez, C. M. Dunham, Mechanism of
680 endonuclease cleavage by the HigB toxin. *Nucleic Acids Res* **44**, 7944-7953 (2016).
681 44. A. Harms, C. Fino, M. A. Sorensen, S. Semsey, K. Gerdes, Prophages and Growth Dynamics
682 Confound Experimental Results with Antibiotic-Tolerant Persister Cells. *mBio* **8** (2017).
683 45. F. Goormaghtigh *et al.*, Reassessing the Role of Type II Toxin-Antitoxin Systems in Formation
684 of Escherichia coli Type II Persister Cells. *mBio* **9** (2018).
685 46. W. T. Chan, M. Espinosa, C. C. Yeo, Keeping the Wolves at Bay: Antitoxins of Prokaryotic
686 Type II Toxin-Antitoxin Systems. *Front Mol Biosci* **3**, 9 (2016).
687 47. H. S. Deter, R. V. Jensen, W. H. Mather, N. C. Butzin, Mechanisms for Differential Protein
688 Production in Toxin-Antitoxin Systems. *Toxins* **9** (2017).
689 48. Q. B. Tian, T. Hayashi, T. Murata, Y. Terawaki, Gene product identification and promoter
690 analysis of hig locus of plasmid Rts1. *Biochem Biophys Res Commun* **225**, 679-684 (1996).
691 49. K. A. Datsenko, B. L. Wanner, One-step inactivation of chromosomal genes in Escherichia
692 coli K-12 using PCR products. *Proc Natl Acad Sci U S A* **97**, 6640-6645 (2000).
693 50. W. Kabsch, Xds. *Acta crystallographica* **66**, 125-132 (2010).
694 51. P. D. Adams *et al.*, PHENIX: a comprehensive Python-based system for macromolecular
695 structure solution. *Acta crystallographica* **66**, 213-221 (2010).
696 52. P. Emsley, B. Lohkamp, W. G. Scott, K. Cowtan, Features and development of Coot. *Acta*
697 *crystallographica* **66**, 486-501 (2010).
698 53. Schrodinger, LLC (2010) The PyMOL Molecular Graphics System, Version 1.3r1.

bioRxiv preprint doi: https://doi.org/10.1101/2021.03.04.434028; this version posted March 5, 2021. The copyright holder for this preprint (which was not certified by peer review) is the author/funder. All rights reserved. No reuse allowed without permission.

699 54. J. Schaefer, G. Jovanovic, I. Kotta-Loizou, M. Buck, Single-step method for beta-
700 galactosidase assays in Escherichia coli using a 96-well microplate reader. *Anal Biochem*
701 **503**, 56-57 (2016).
702 55. I. Y. B.-S. D.A. Case, S.R. Brozell, D.S. Cerutti, T.E. Cheatham, III, V.W.D. Cruzeiro, T.A.
703 Darden, R.E. Duke, D. Ghoreishi, M.K. Gilson, H. Gohlke, A.W. Goetz, D. Greene, R Harris,
704 N. Homeyer, Y. Huang, S. Izadi, A. Kovalenko, T. Kurtzman, T.S. Lee, S. LeGrand, P. Li, C.
705 Lin, J. Liu, T. Luchko, R. Luo, D.J. Mermelstein, K.M. Merz, Y. Miao, G. Monard, C. Nguyen,
706 H. Nguyen, I. Omelyan, A. Onufriev, F. Pan, R. Qi, D.R. Roe, A. Roitberg, C. Sagui, S. Schott-
707 Verdugo, J. Shen, C.L. Simmerling, J. Smith, R. SalomonFerrer, J. Swails, R.C. Walker, J.
708 Wang, H. Wei, R.M. Wolf, X. Wu, L. Xiao, D.M. York and P.A. Kollman (2018) AMBER 2018.
709 (University of California, San Francisco).
710 56. J. A. Maier *et al.*, ff14SB: Improving the Accuracy of Protein Side Chain and Backbone
711 Parameters from ff99SB. *J Chem Theory Comput* **11**, 3696-3713 (2015).
712 57. R. Galindo-Murillo *et al.*, Assessing the Current State of Amber Force Field Modifications for
713 DNA. *J Chem Theory Comput* **12**, 4114-4127 (2016).
714 58. W. L. Jorgensen, J. Chandrasekhar, J. D. Madura, R. W. Impey, M. L. Klein, Comparison of
715 simple potential functions for simulating liquid water. *J. Chem. Phys.* **79** (1983).
716 59. R. Salomon-Ferrer, A. W. Gotz, D. Poole, S. Le Grand, R. C. Walker, Routine Microsecond
717 Molecular Dynamics Simulations with AMBER on GPUs. 2. Explicit Solvent Particle Mesh
718 Ewald. *J Chem Theory Comput* **9**, 3878-3888 (2013).
719 60. S. Le Grand, A. W. Gotz, R. C. Walker, SPFP: Speed without compromise—A mixed
720 precision model for GPU accelerated molecular dynamics simulations. *Computer Physics*
721 *Communications* **184**, 374-380 (2013).
722 61. J. C. Ryckaert, G.; Berendsen, H.J.C., Numerical integration of the cartesian equations of
723 motion of a system with constraints: molecular dynamics of n-alkanes. *Journal of*
724 *Computational Physics* **23**, 327-341 (1977).

bioRxiv preprint doi: https://doi.org/10.1101/2021.03.04.434028; this version posted March 5, 2021. The copyright holder for this preprint (which was not certified by peer review) is the author/funder. All rights reserved. No reuse allowed without permission.

725 62. D. R. Roe, T. E. Cheatham, 3rd, PTRAJ and CPPTRAJ: Software for Processing and Analysis
726 of Molecular Dynamics Trajectory Data. *J Chem Theory Comput* **9**, 3084-3095 (2013).

727
728
729
730
731
732
733
734
735
736
737
738
739
740
741
742
743
744
745
746
747
748
749

bioRxiv preprint doi: https://doi.org/10.1101/2021.03.04.434028; this version posted March 5, 2021. The copyright holder for this preprint (which was not certified by peer review) is the author/funder. All rights reserved. No reuse allowed without permission.

750 **FIGURES**

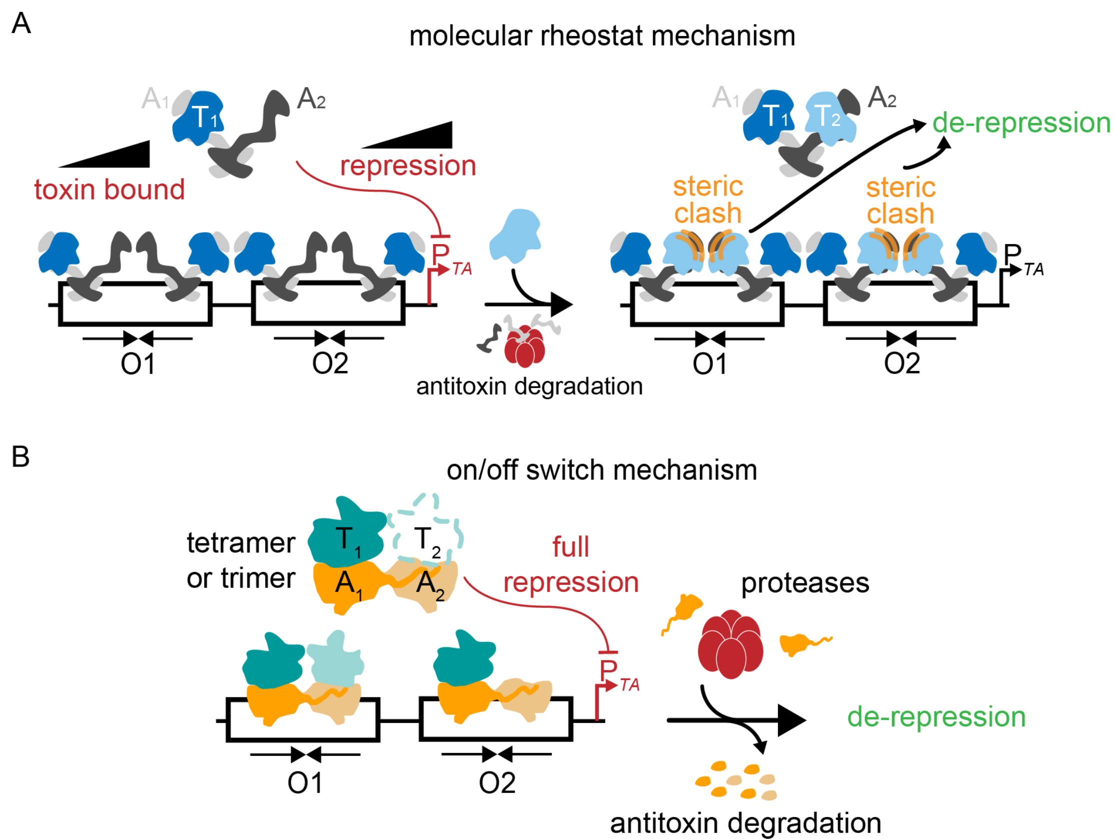

751

752 **Figure 1. Diverse transcriptional control mechanisms that regulate expression of**
753 **toxin-antitoxin complexes.** Toxin (T) and antitoxin (A) proteins form multimeric complexes
754 that bind operator sites (O1 and O2) that overlap with their promoters (P_{TA}) to repress
755 transcription. (**A**) In some type II toxin-antitoxin systems, changing levels of toxins (due to
756 antitoxin proteolysis) that bind to the repressor complex leads to steric clashes and/or
757 changes in affinity causing de-repression. In this case, the system functions as a molecular
758 rheostat responsive to toxin levels. (**B**) In contrast, other toxin-antitoxin systems are not
759 sensitive to changes in toxin concentrations and thus function as on/off transcriptional
760 switches dependent on antitoxin depletion from proteolysis.

761

762

bioRxiv preprint doi: https://doi.org/10.1101/2021.03.04.434028; this version posted March 5, 2021. The copyright holder for this preprint (which was not certified by peer review) is the author/funder. All rights reserved. No reuse allowed without permission.

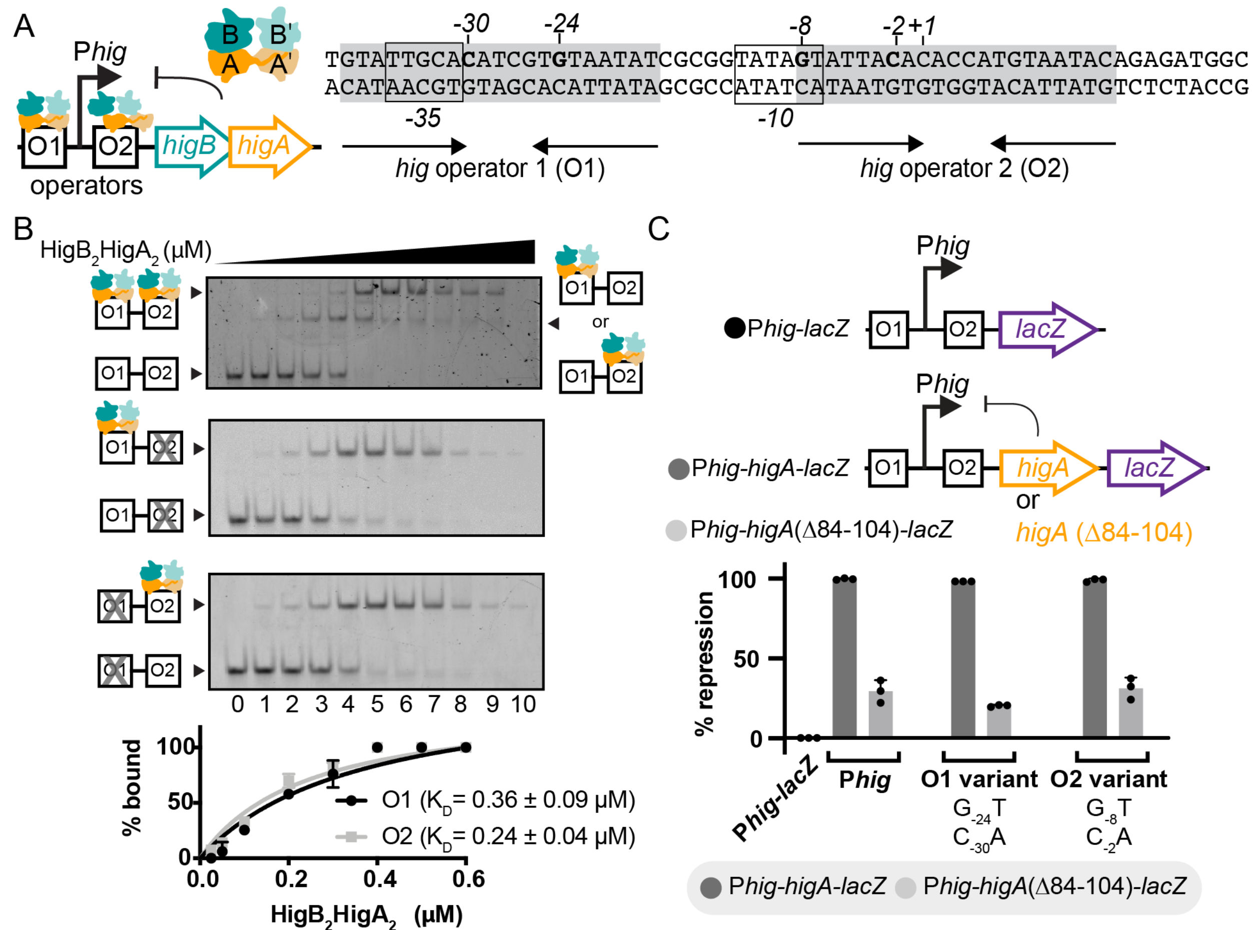

763

764 **Figure 2. Binding of $HigB_2HigA_2$ to a single operator is sufficient for transcriptional**
765 **repression of the *hig* operon.** (**A**) *Left*, organization of the *hig* operon containing the
766 operators O1 and O2, the P*hig* promoter, *higB* toxin and *higA* antitoxin genes. *Right*, the
767 nucleotide sequences of O1 and O2, with the +1 transcriptional start site and the -35 and -
768 10 sites indicated. The sequence recognized by HigA is shown in grey and operator
769 nucleotides C_{-30}, G_{-24}, G_{-8}, and C_{-2} important for HigA binding are shown in bold. (**B**) EMSA
770 of $HigB_2HigA_2$ binding to wild-type P*hig* (top), O1 only (O2 scrambled; middle), and O2 only
771 (O1 scrambled; bottom) DNA. Band intensities were plotted from EMSAs as the percent of
772 $HigB_2HigA_2$ bound to DNA versus $HigB_2HigA_2$ (concentrations used: 0, 0.025, 0.05, 0.1, 0.2,
773 0.3, 0.4, 0.5, 0.6, 0.7, 0.8 μM). Curves represent the fit from which K_Ds were calculated. (**C**)
774 β-gal assays of *E. coli* BW25113 transformed with pQF50-P*hig-lacZ* (black), pQF50-P*hig*-

bioRxiv preprint doi: https://doi.org/10.1101/2021.03.04.434028; this version posted March 5, 2021. The copyright holder for this preprint (which was not certified by peer review) is the author/funder. All rights reserved. No reuse allowed without permission.

775 *higA-lacZ* (dark grey), or pQF50-P*hig-higA*(Δ84-104)-*lacZ* (light grey). Each operator site
776 was tested using known operator mutations of either O1 ($G_{-24}T$, $C_{-30}A$) or O2 ($G_{-7}T$, $C_{-2}A$)
777 (38).
778
779
780
781
782
783
784
785
786
787
788
789
790
791
792
793
794
795
796
797
798
799

bioRxiv preprint doi: https://doi.org/10.1101/2021.03.04.434028; this version posted March 5, 2021. The copyright holder for this preprint (which was not certified by peer review) is the author/funder. All rights reserved. No reuse allowed without permission.

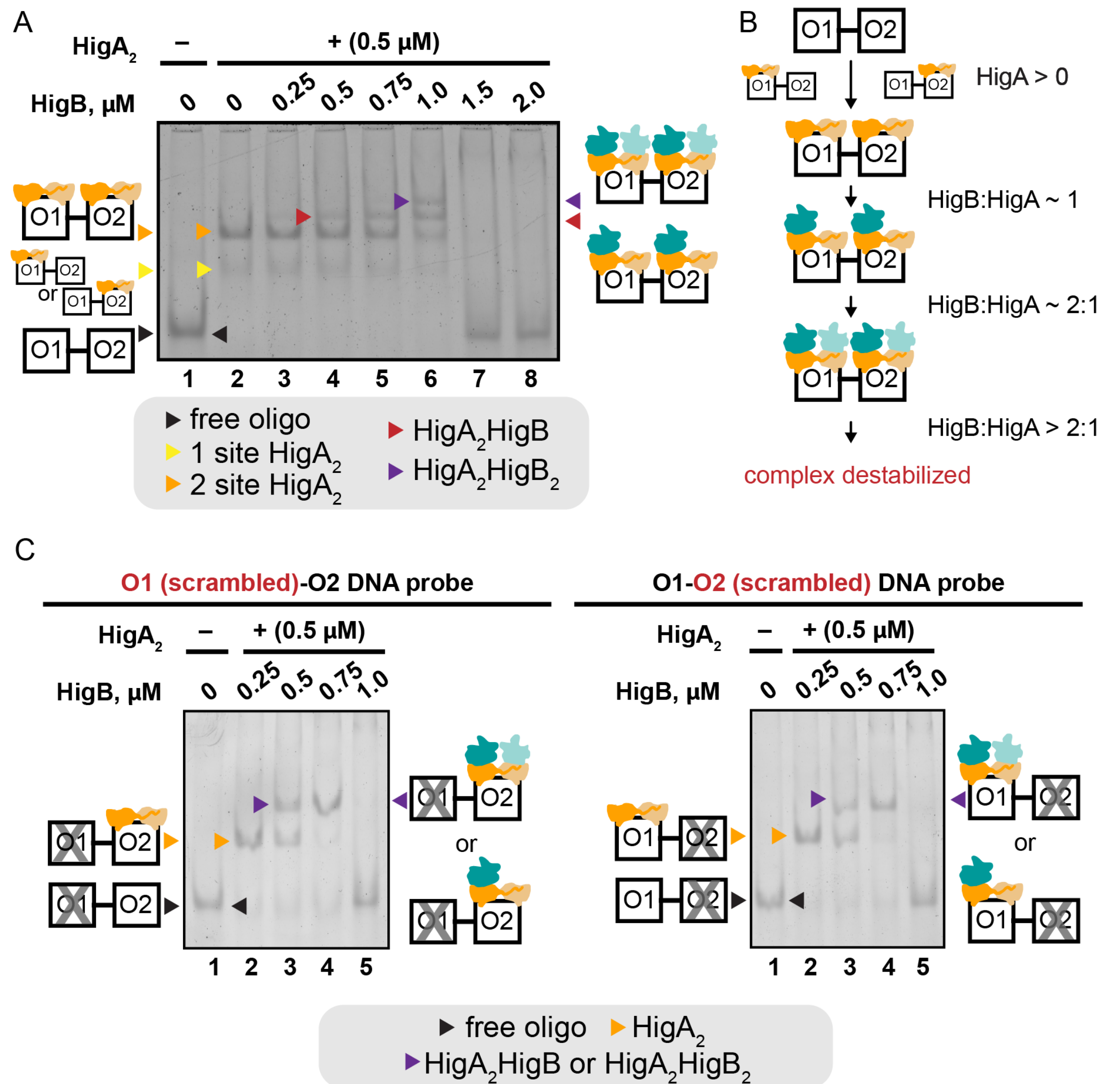

800

801 **Figure 3. Formation of higher oligomeric states upon addition of HigB to the HigA-**
802 **DNA complex.** (**A**) EMSA of HigB addition to the $HigA_2$-O1-O2 DNA complex. The O1-O2
803 DNA migrates the fastest (lane 1, black arrowhead) and incubation with the 0.5 μM $HigA_2$
804 dimer results in a retardation of O1-O2 to form two shifts (lane 2, yellow and orange
805 arrowheads). Increasing amounts of HigB results in the formation of higher molecular weight
806 complexes (lanes 3-6, red and purple arrowheads). When the molar ratio of HigB to HigA
807 exceeds 1 (>1.0 μM HigB for 0.5 μM $HigA_2$ dimer), the high molecular weight shifts are no
808 longer observed indicating that neither HigA nor HigB binds. (**B**) Schematic of the different

bioRxiv preprint doi: https://doi.org/10.1101/2021.03.04.434028; this version posted March 5, 2021. The copyright holder for this preprint (which was not certified by peer review) is the author/funder. All rights reserved. No reuse allowed without permission.

809 HigBHigA-O1-O2 DNA complexes formed with changing the HigB:HigA ratio. Multiple
810 oligomeric arrangements are possible in the case of a trimeric $HigA_2HigB$ complex but only
811 one example is shown. (**C**) EMSA of HigB addition to the $HigA_2$-O1-O2 DNA complex when
812 either O1 or O2 is scrambled. O1-O2 DNA migrates the fastest (lane 1, black arrowhead)
813 and incubation with the $HigA_2$ dimer results in a retardation of O1-O2 to form two shifts (lane
814 2, orange arrowhead). The addition of HigB results in the formation of higher molecular
815 weight complexes (lane 3, purple arrowhead) with a molar excess of HigB over HigA causes
816 the scrambled DNA probe to be released (lane 5).
817
818
819
820
821
822
823
824
825
826
827
828
829
830
831
832
833

bioRxiv preprint doi: https://doi.org/10.1101/2021.03.04.434028; this version posted March 5, 2021. The copyright holder for this preprint (which was not certified by peer review) is the author/funder. All rights reserved. No reuse allowed without permission.

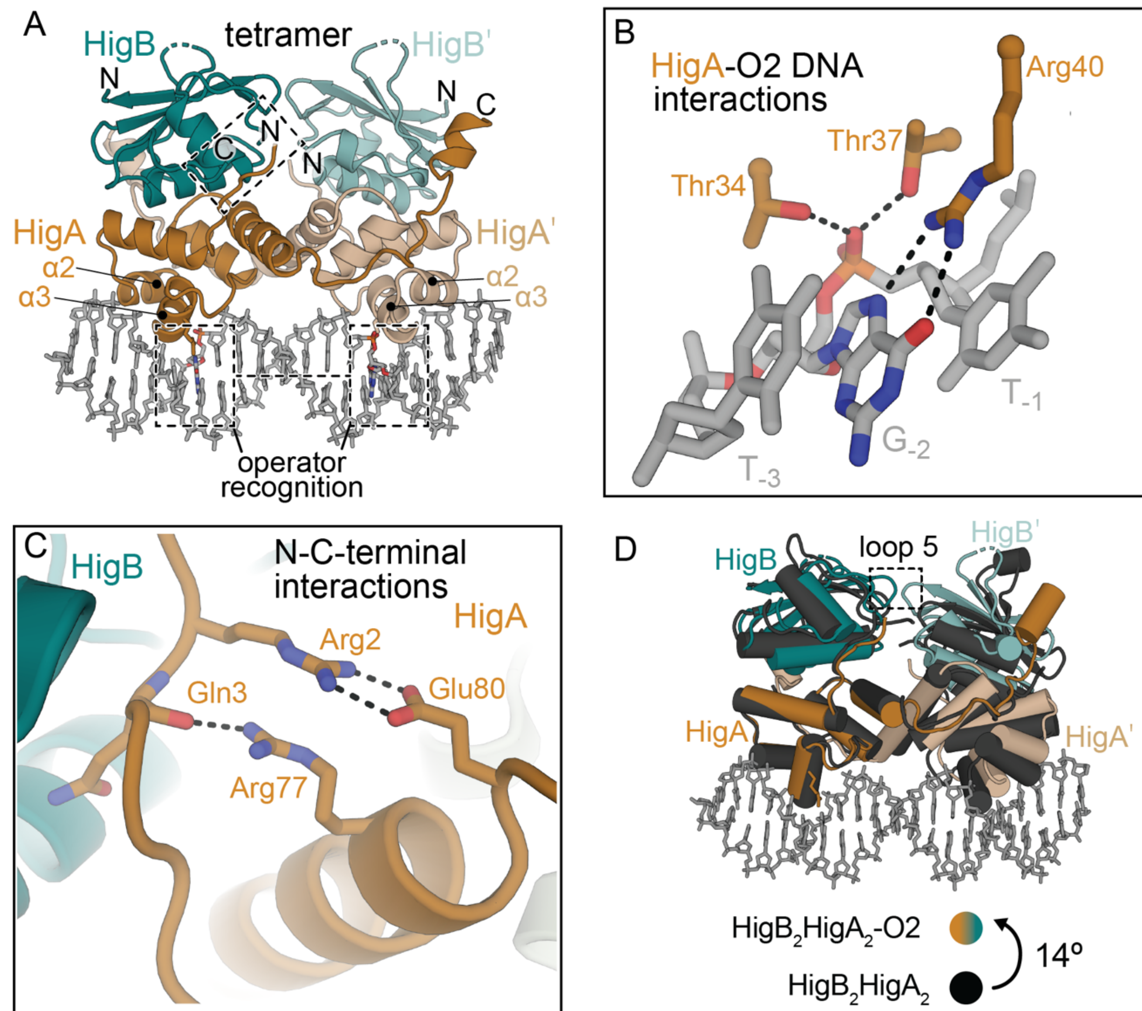

834

835 **Figure 4. Structure of tetrameric $HigB_2HigA_2$ bound to O2 DNA.** (**A**) The 2.4-Å structure
836 of tetrameric $HigB_2HigA_2$-O2 DNA complex (PDB code 6W6U). HigA recognizes the T_{-1}, G_{-2},
837 T_{-3}, A_{-4} DNA operator region via α2 and α3. N and C-terminal regions of HigA are boxed. (**B**)
838 HigA Arg40 makes the only sequence specific interactions with the nucleobase of G_{-2} while
839 HigA residues Thr34 and Thr37 (both from α3) stably interact with the phosphate of G_{-2}. (**C**)
840 The N- and C-terminal residues of HigA become ordered upon both HigB binding. HigA
841 residue Arg77 forms a hydrogen bond with the backbone carbonyl of Gln3 and Arg2 and
842 Glu80 interact via a salt bridge. (**D**) Comparison of the tetrameric $HigB_2HigA_2$ complex (all
843 black; PDB code 4MCX) and $HigB_2HigA_2$-O2 DNA complex (PDB code 4MCX) reveal a ~14º
844 rotation of $HigB_2HigA_2$ away from DNA that allows recognition.

bioRxiv preprint doi: https://doi.org/10.1101/2021.03.04.434028; this version posted March 5, 2021. The copyright holder for this preprint (which was not certified by peer review) is the author/funder. All rights reserved. No reuse allowed without permission.

845

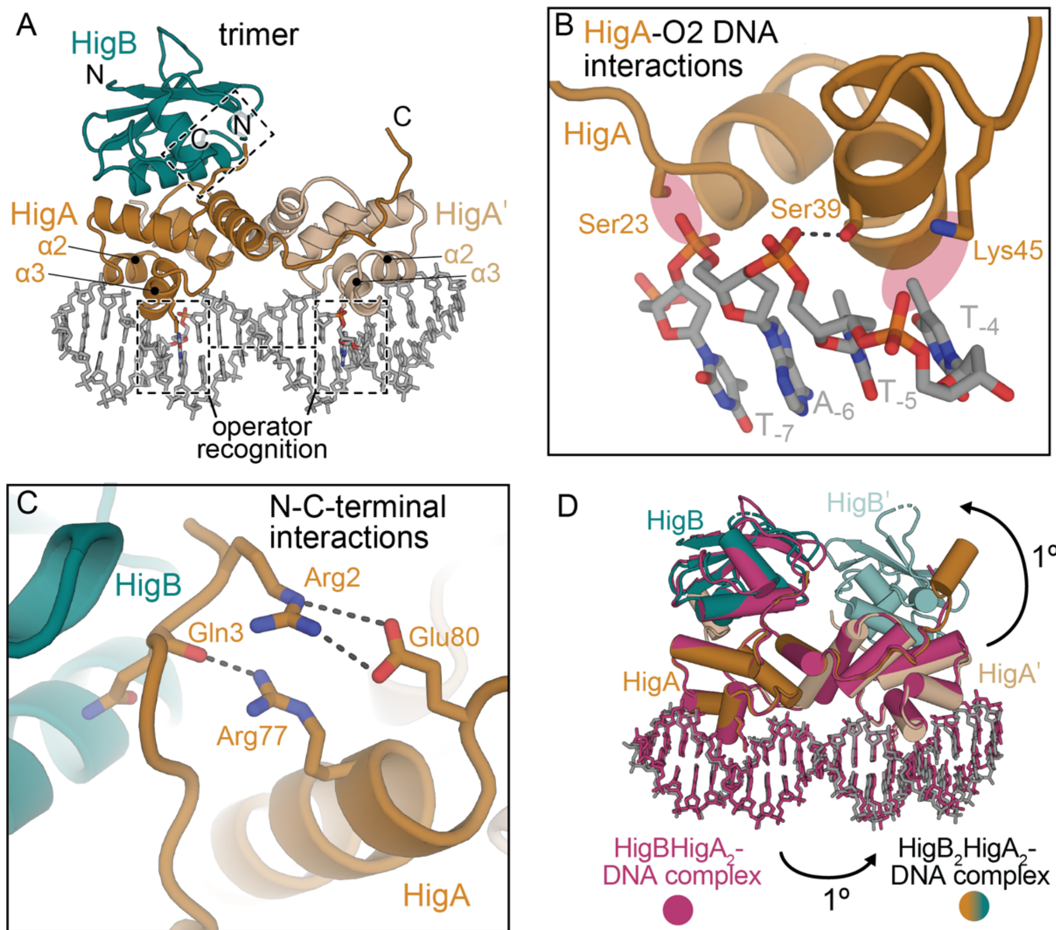

846

847 **Figure 5. Structure of trimeric HigBHigA$_2$ bound to O2 DNA.** The 2.8-Å structure of
848 trimeric HigBHigA$_2$-O2 DNA (PDB code 6WFP). HigA recognizes the T_{+6}, G_{+7}, T_{+8}, A_{+9} DNA
849 region via α2 and α3. N and C-terminal regions of HigA are boxed. (**B**) In the HigB$_2$HigA$_2$-
850 O2 DNA structure (PDB code 6W6U), HigA residues Ser23, Ser39, and Lys45 interact with
851 the backbone phosphate of T_{-7}, T_{-5}, and T_{-4} respectively to rigidify the T_{-1}, G_{-2}, T_{-3}, A_{-4}
852 sequence for nucleotide-specific recognition on the opposite strand. In the trimeric
853 HigBHigA$_2$-O2 structure, only Ser39 interacts with the phosphate backbone and Ser23 and
854 Lys45 are too distant (red highlighted region). (**C**) The N- and C-terminal residues of HigA
855 become ordered upon a single HigB monomer binding similar to when two HigB monomers
856 bind (Fig. 4C). (**D**) Comparison of trimeric HigBHigA$_2$-O2 DNA (pink; PDB code 6WFP) and

bioRxiv preprint doi: https://doi.org/10.1101/2021.03.04.434028; this version posted March 5, 2021. The copyright holder for this preprint (which was not certified by peer review) is the author/funder. All rights reserved. No reuse allowed without permission.

857 tetrameric $HigB_2HigA_2$-O2 DNA (PDB code 6W6U) are incredibly similar with an r.m.s.d of
858 0.7 Å (for 1479 equivalent atoms) and less than a ~1° rotation.
859
860
861
862
863
864
865
866
867
868
869
870
871
872
873
874
875
876
877
878
879
880
881

bioRxiv preprint doi: https://doi.org/10.1101/2021.03.04.434028; this version posted March 5, 2021. The copyright holder for this preprint (which was not certified by peer review) is the author/funder. All rights reserved. No reuse allowed without permission.

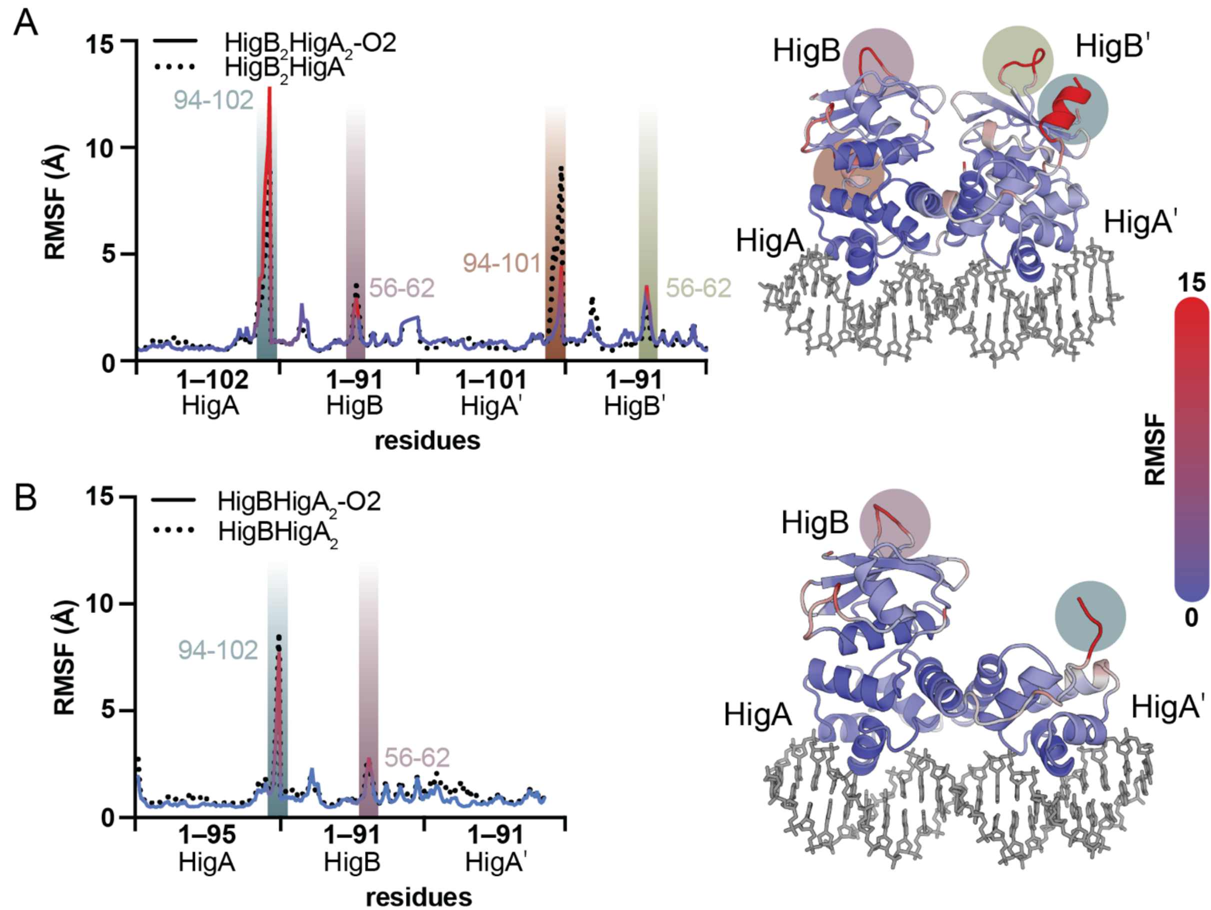

882

883 **Figure 6. Trimeric $HigBHigA_2$ and tetrameric $HigB_2HigA_2$ exhibit similar dynamics in**
884 **the presence or absence of O2 DNA.** Root-mean-square-fluctuations (RMSFs) of Cα
885 atoms for each residue in the (**A**) $HigBHigA_2$ or (**B**) $HigB_2HigA_2$ complexes are calculated
886 from 1 ms MD trajectories. Regions that have increased RMSFs are indicated with
887 highlighted bars that correspond to their positions on the HigBHigA-O2 structures (*right*).
888 High RMSF spikes correlate to either labile C-termini of HigA or HigB loop regions with
889 colored circles corresponding to the highlighted bars on the left.

890

bioRxiv preprint doi: https://doi.org/10.1101/2021.03.04.434028; this version posted March 5, 2021. The copyright holder for this preprint (which was not certified by peer review) is the author/funder. All rights reserved. No reuse allowed without permission.

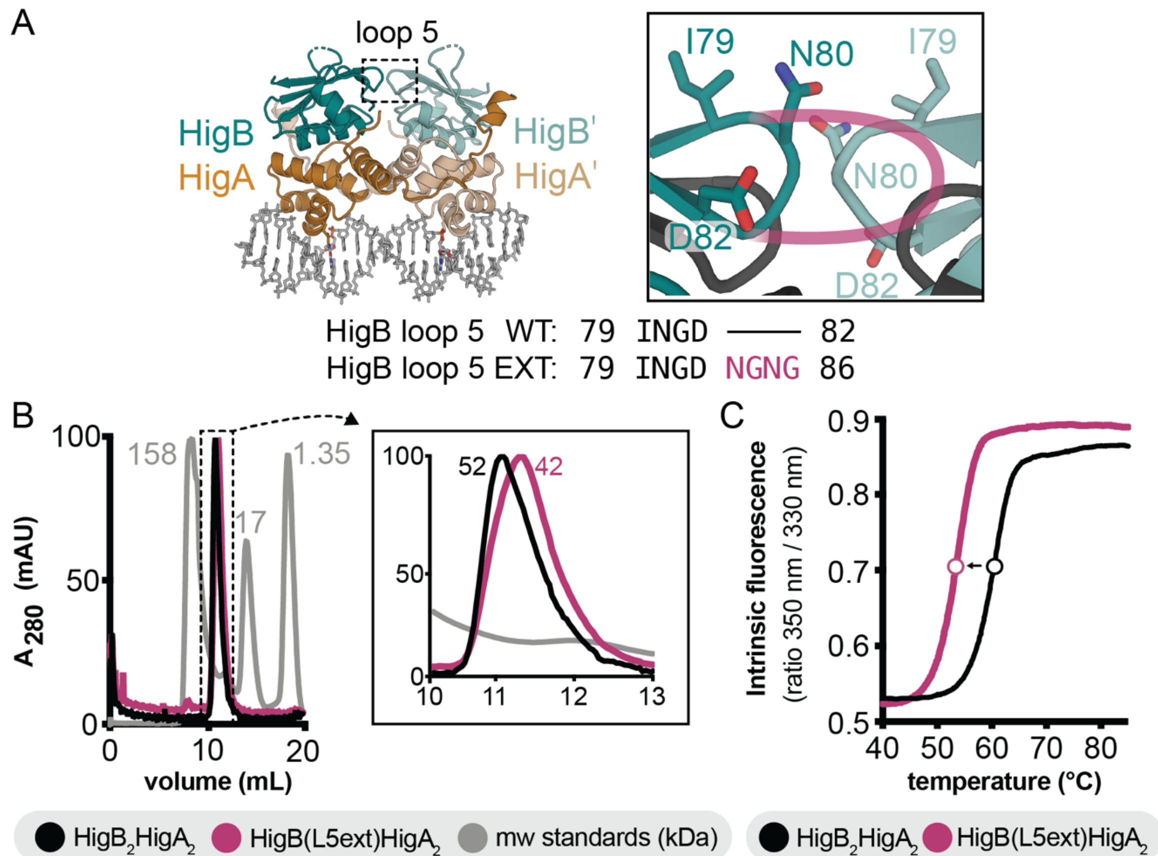

891

892 **Figure 7. Engineering a trimeric HigBHigA$_2$ complex.** (**A**) To prevent two HigB monomers
893 from binding, loop 5 (L5) of HigB was extended by the insertion of four residues (Asn, Gly,
894 Asn, Gly; NGNG; "L5ext", magenta) after residue Asp82. The dotted box indicating the L5
895 region of two HigB monomers is zoomed in (*right*). The theoretical extension of L5 is shown
896 in magenta with the wild-type HigB and HigB(L5ext) amino acid alignment shown
897 underneath. (**B**) Size exclusion chromatography of purified wild-type HigB$_2$HigA$_2$ shows an
898 elution volume that corresponds to a molecular weight of 52 kDa. HigB(L5ext)HigA$_2$ complex
899 (magenta) elutes at a volume corresponding to a molecular weight of 42 kDa with the inset
900 showing a zoomed in view. Molecular weight standards are shown in grey. (**C**) Nano-DSF
901 analysis of wild-type HigB$_2$HigA$_2$ (black) and HigB(L5ext)HigA$_2$ (magenta) shows that the
902 HigB(L5ext)HigA$_2$ complex has ~5ºC lower T_i value than HigB$_2$HigA$_2$. Fluorescence values

bioRxiv preprint doi: https://doi.org/10.1101/2021.03.04.434028; this version posted March 5, 2021. The copyright holder for this preprint (which was not certified by peer review) is the author/funder. All rights reserved. No reuse allowed without permission.

903 were normalized to the highest tested temperature and the boundary of each line represents
904 the mean ± SD of values of three independent experiments.
905
906
907
908
909
910
911
912
913
914
915
916
917
918
919
920
921
922
923
924
925
926
927

bioRxiv preprint doi: https://doi.org/10.1101/2021.03.04.434028; this version posted March 5, 2021. The copyright holder for this preprint (which was not certified by peer review) is the author/funder. All rights reserved. No reuse allowed without permission.

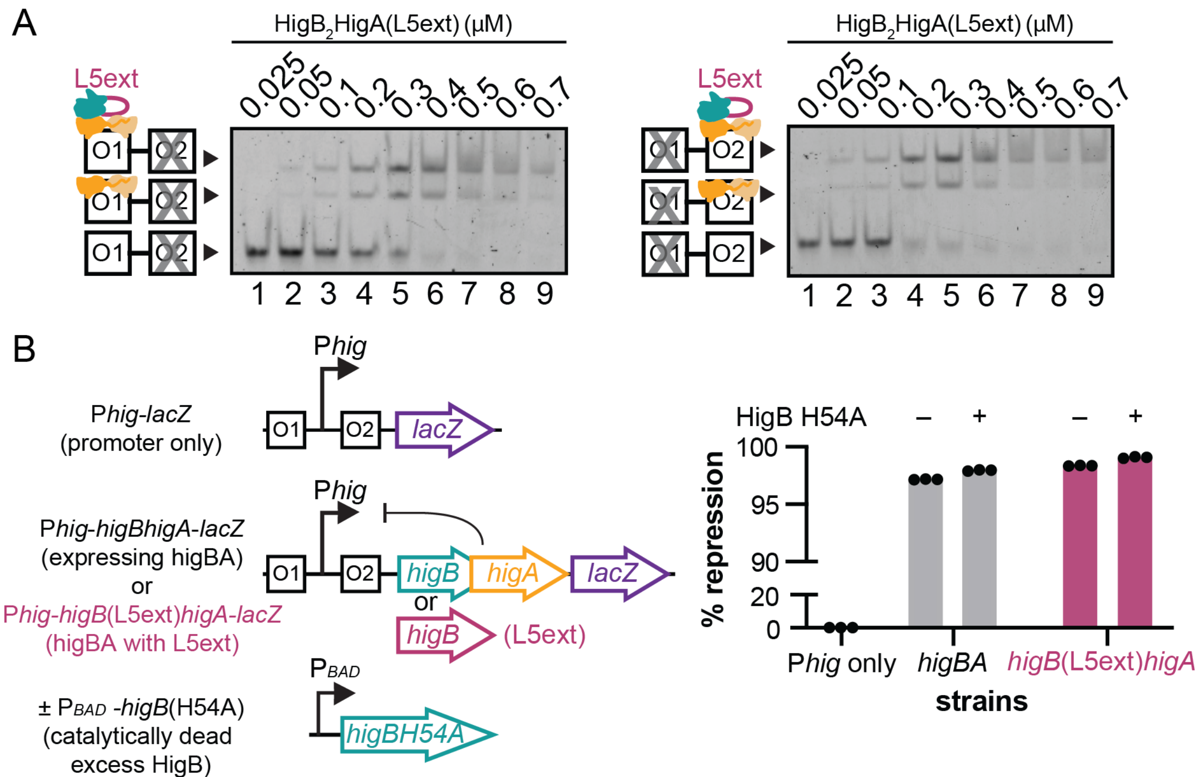

928

929 **Figure 8. Trimeric HigB(L5ext)HigA$_2$ is sufficient to repress transcription of P*hig*.** (**A**)
930 EMSA of HigB(L5ext)HigA$_2$ binding to O1 DNA (O2 scrambled; *left*) or to O2 DNA (O1
931 scrambled; *right*). (**B**) β-gal assays of *E. coli* BW25113 transformed with either pQF50-P*hig*-
932 *lacZ* (P*hig* only), pQF50-P*hig-higBhigA-lacZ* (*higBhigA*), pQF50-P*hig-higB*(L5ext)*higA-lacZ*
933 (*higB*(L5ext)*higA*), and/or pBAD33-*higB*(H54A). P*hig* only demonstrates the maximum
934 amount of β-gal activity (black bar, 0% repression). Constructs containing either a wild-type
935 HigBHigA (grey bars) or a HigB(L5ext)HigA variant (pink bars) both repress transcription
936 (first bar in each group). Excess HigB expression (using a catalytically inactive H54A variant)
937 results in little difference in repression (second bars). Error bars represent the mean ± SD
938 of values of three independent experiments (raw values shown as dots).

939

940